de Oliveira Gabriel (Orcid ID: 0000-0002-1940-6874)

Effects of land-cover changes on the partitioning of surface energy and water fluxes in Amazonia using high-resolution satellite imagery

Land-cover changes and water fluxes in Amazonia using satellite imagery

Gabriel de Oliveira[1*], Nathaniel A. Brunsell[1], Elisabete C. Moraes[2], Yosio E. Shimabukuro[2], Thiago V. dos Santos[3], Celso von Randow[2], Renata G. de Aguiar[4], Luiz E. O. C. Aragao[2,5]

[1]Department of Geography and Atmospheric Science, University of Kansas, 1475 Jayhawk Boulevard, Lawrence, KS 66045, USA

[2] Brazilian National Institute for Space Research, 1758 Astronautas Avenue, Sao Jose dos Campos, SP 12227-010, Brazil

[3]Department of Climate and Space Sciences and Engineering, University of Michigan, 2455 Howard Street, Ann Arbor, MI 48109, USA

[4]Department of Environmental Engineering, Federal University of Rondonia, Ji-Parana, RO 76900-726, Brazil

[5]College of Life and Environmental Sciences, University of Exeter, Rennes Drive, Exeter, EX4 4RJ, UK

* Corresponding author:

Gabriel de Oliveira (gabrieloliveira@ku.edu)

Address: Department of Geography and Atmospheric Science, University of Kansas, 1475 Jayhawk Boulevard, Lawrence, KS 66045, USA

Tel: +1 (785) 727-8974

Abstract

Spatial variability of surface energy and water fluxes at local scales is strongly controlled by soil and micrometeorological conditions. Thus, the accurate estimation of these fluxes from space at high spatial resolution has the potential to improve prediction of the impact of land-use changes on the local environment. In this study, Advanced Spaceborne Thermal Emission and Reflection Radiometer (ASTER) and Large-Scale Biosphere-Atmosphere Experiment in Amazonia (LBA) data were used to examine the partitioning of surface energy and water fluxes over different land cover types in one wet year (2004) and one drought year (2005) in eastern Rondonia state, Brazil. The spatial variation of albedo, net radiation (Rn), soil (G) and sensible (H) heat fluxes, evapotranspiration (ET), and evaporative fraction (EF) were primarily related to the lower presence of forest (primary (PF) or secondary (SF)) in the western side of the Ji-Parana river in comparison with the eastern side, located within the Jaru Biological Reserve protected area. Water limitation in this part of Amazonia tends to affect

anthropic (pasture (PA) and agriculture (AG)) ecosystems more than the natural land covers (PF and SF). We found statistically significant differences on the surface fluxes prior to and ~1-year after the deforestation. Rn over forested areas is ~10% greater in comparison with PA and AG. Deforestation and consequent transition to PA or AG increased the total energy (~200-400%) used to heat the soil subsurface and raise air temperatures. These differences in energy partitioning contributed to approximately three times higher ET over forested areas in comparison with non-forested areas. The conversion of PF to AG is likely to have a higher impact in the local climate in this part of Amazonia when compared to the change to PA and SF, respectively. These results illustrate the importance of conserving secondary forest areas in Amazonia.

Keywords: Amazonia, evapotranspiration, spatial variation, land cover changes, ASTER images.

1. Introduction

The Amazon region concentrates the largest rainforest in the world, acting as a major source of heat and water vapor for the global atmosphere (Gash et al., 2004; Davidson et al., 2012; Aragao et al., 2014). Previous studies have shown that deforestation in the Amazon can lead to changes in surface net radiation (Rn), resulting in higher or lower availability of energy for the evapotranspiration (ET) processes (Malhi et al., 2002; Stark et al., 2016). However, in order to better understand the

impacts caused by land cover changes it is necessary to obtain detailed information on the partitioning of surface fluxes. From this information, it is possible to analyze the ecohydrological mechanisms of different ecosystems and their biological responses to the processes of water cycling (Scott et al., 2003; Christoffersen et al., 2014). Here, we highlight that alterations on flux partitioning over the Amazon can influence the atmospheric circulation and precipitation (PPT) in the tropics (Swann et al., 2012; Zanchi et al., 2015).

For more than 20 years, field experiments have been developed for acquiring micrometeorological data in Amazonia (Malhi et al., 2002; Zeri et al., 2014). These data have been used primarily as input in global and regional models, providing valuable information to develop the knowledge about the Amazon in the fields of climate physics, ecohydrology and biogeochemistry (Gonçalves et al., 2013; Broedel et al., 2017). However, two issues regarding these data should be noted: (1) measurements obtained by such experiments are usually local and representative of small areas, and (2) most of the field sites are located over primary forest areas and therefore not representative of the current spatial variation of land cover in the region (de Oliveira et al., 2017). An example of this spatial heterogeneity is the state of Rondonia, located in the Brazilian Amazon, now dominated by larger deforested patches. Beginning in 1970, Rondonia had been the site of a series of government settlement programs. For this reason, it is possible to observe extensive patches of different land cover types as pasture, annual crops, secondary succession forest, among others (Pedlowski et al., 1997; Frohn and Hao, 2006). Several micrometeorological and numerical modeling

studies have been conducted using Rondonia as a case study (von Randow et al., 2004; Hasler and Avissar, 2007; Butt et al., 2011; Khanna et al., 2017).

The relevance of physical phenomena related to energy and water exchanges between the surface and atmosphere under climate change leads to the need for studies at more refined spatial scales (Bonan, 2008; El-Masri et al., 2013). This would facilitate representation of the spatial heterogeneity in global and regional models. As mentioned before, most of the observational studies in the Amazon region have been performed over primary forest areas. One way to extend such analyses to the diverse ecosystems of the Amazon is the use of surface energy balance models combining micrometeorological measurements and remote sensing data. Surface energy balance models differ according to the input data, assumptions and accuracy of the results (Ruhoff et al., 2013). However, a common aspect among the algorithms are the satellite input data, once all algorithms require information regarding the visible, near infrared and thermal infrared spectral regions (Li et al., 2009; Yang et al., 2012; French et al., 2015). The primary estimates from such models are related to albedo, Rn, soil heat flux (G), sensible heat flux (H), ET, and evaporative fraction (EF) (Gowda et al., 2008; Bhattarai et al., 2012).

Studies using this approach have been developed in the Amazon region, but most of them make use of satellite data with medium and low spatial resolution (30 m to 1 km) (Santos et al., 2011; de Oliveira and Moraes, 2013; de Oliveira et al., 2016; Khand et al., 2017; Numata et al., 2017; de Oliveira et al., 2017). The main requirement for surface energy balance modeling is the ability to distinguish land cover types that

have different mass and heat transfer characteristics and resolve spatial variability of the considered processes within a land-class type (French et al., 2005). Spatial variability of surface energy and water fluxes at local scales is strongly controlled by soil and micrometeorological conditions. Thus, the accurate estimation of these fluxes from space at high spatial resolution has the potential to improve prediction of the impact of land-use changes on the local environment. The Advanced Spaceborne Thermal Emission and Reflection Radiometer (ASTER), launched in 1999 onboard the NASA's Terra satellite, was developed to establish a spaceborne capability for high spatial (15 m), multispectral visible, near infrared and thermal infrared remote sensing data mapping of the Earth's environment (Fujisada et al., 2005; Abrams et al., 2015). Previously, only select images over the USA and its Territories were publicly available. In 2016, the Land Processes Distributed Active Archive Center (LPDAAC) began distributing ASTER data over the entire globe. The unlimited public access of this type of data provides a unique opportunity to estimate surface biophysical and hydrological variables over the globe with high spatial resolution.

Based on the considerations above, this study aims to investigate the partitioning of surface energy and water fluxes over different land cover types in one wet year (2004) and one drought year (2005) in the eastern flank of Rondonia combining ASTER images and flux tower observations from the Large-Scale Biosphere-Atmosphere Experiment in Amazonia (LBA). More specifically, we aim to (1) analyze albedo, Rn, G, H, ET, and EF for different land cover types, and (2) assess the effects of local land-cover changes on the surface fluxes.

2. Materials and methods

2.1 Study area and flux tower site

The study area is located in the eastern flank of the state of Rondonia, Brazil, southwestern Amazonia (Figure 1). The study area covers 887.1 km^2, ranging in elevation between 100 and 150 m above sea level. The predominant climate is equatorial, warm and moist, with annual rainfall and air temperature varying between 1400 to 2400 mm and 22°C to 27°C, respectively. The southern hemisphere summer (December to February) is the rainiest period in the region with monthly totals over 200 mm. During the dry season (June to August), it is common to observe several weeks without rain (von Randow et al., 2004).

Soils in the region are classified primarily as medium textured red-yellow podzols (Alvala et al., 2002). The main natural vegetation type in the study area is the dense tropical forest. However, it has been logged and substantially perturbed in the past few decades. We note that part of the study area is inside of the Jaru Biological Reserve (JBR), which is administrated by the Brazilian Environmental Protection Agency (IBAMA). As can be seen in Figure 1, the JBR is located along the eastern flank of the Ji-Parana river.

The eddy flux tower data used in this study (hereafter referred to as JBR flux tower) is part of the LBA project and is located inside the JBR over an undisturbed

tropical forest. The canopy has a mean height of 35 m, with some of the taller trees reaching up to 45 m (Andreae et al., 2002). The JBR flux tower is 64 m tall and is located 120 m above sea level at the geographic coordinates 10.19°S and 61.87°W (de Oliveira and Moraes, 2013).

(Figure 1)

2.2 Surface data

The data collected at the JBR flux tower for 2004-2005 were acquired from the LBA Rondonia Regional Office (Ji-Parana, RO, Brazil, http://lba2.inpa.gov.br/). Flux tower measurements were used as input and validation data in the Surface Energy Balance Algorithm for Land (SEBAL) model (Bastiaanssen et al., 1998a,b). We utilized the following variables: PPT (mm), air temperature (T_{air}) (ºC), wind speed (Ws) (m s^{-1}), incoming (K↓) and outgoing (K↑) shortwave radiation (W m^{-2}), Rn (W m^{-2}), H (W m^{-2}), and latent heat flux (LE) (W m^{-2}). LE was converted to ET (mm) by dividing it by the latent heat of vaporization (λ=2.45x10^6 J kg^{-1}). The surface albedo was calculated as the ratio of the outgoing to the incoming shortwave radiation.

The LBA flux data have been processed according to a common protocol and are aggregated to a half-hourly time step (von Randow et al., 2004; Restrepo-Coupe et al., 2013). The quality control in the data followed a methodology that is applied to all LBA datasets and can be found in Gonçalves et al. (2013) and Restrepo-Coupe et al. (2013).

Gaps in the measurements were filled using the marginal distribution sampling (MDS) method as described in Reichstein et al. (2005). For comparison with instantaneous satellite overpass measurements (~10:30 a.m. local time), we used flux tower data corresponding to 11:00 a.m., consisting of the average values made between 10:30 a.m. and 11:00 a.m. local time in Rondonia state (GMT-4).

2.3 ASTER data

Remote sensing data used in this study were derived from the ASTER sensor aboard the Terra satellite, launched in December 1999 (Yamaguchi et al., 1998). The ASTER sensor has a sun-synchronous near-polar orbit and the daytime repeat visit interval is 16 days at the equator. ASTER operates in the visible through thermal infrared portions of the electromagnetic spectrum (Abrams et al., 2015). Detailed information about the ASTER instrument characteristics can be obtained in Table 1.

The ASTER data were obtained from the NASA Earth Observing System Data and Information System (EOSDIS) (Sioux Falls, SD, USA, https://earthdata.nasa.gov/). We used the following version 3 products: AST07XT and AST08. AST07XT provides surface reflectance for bands 1-9 and AST08 gives land surface temperature (LST). We used the data acquired on 16 June 2004 and 5 July 2005 at 10:32:11 a.m. and 10:31:44 a.m. local time, respectively. It is important to note here that the scenes used in the study were the only ones free of cloud cover and which had all ASTER detectors working properly throughout the full record of ASTER data acquisition (~18 years) in

the study area. The SWIR and TIR bands were spatially resampled to 15 m using the nearest neighborhood method (Parker et al., 1983; Lu and Weng, 2006; Hais and Kucera, 2009). The VNIR images were used to co-register the SWIR and TIR images by identifying similar elements in the images. 20 control points were utilized, and a root mean square error of 0.05 was obtained. We chose to upscale the TIR and SWIR data to 15 m in order to have more homogeneous plots for the land cover change analysis (section 2.4), especially for the agricultural and pasture areas.

(Table 1)

2.4 Land-cover

Land cover data from the TerraClass project (Belem, PA, Brazil, http://www.inpe.br/cra/ingles/project_research/terraclass.php) were used in order to analyze the dynamics of the surface energy and water fluxes over different ecosystems in the study area. Begginning in 2004, the TerraClass project has developed five detailed land cover maps for the Brazilian Amazon (2004, 2008, 2010, 2012, and 2014) (Almeida et al., 2016). The TerraClass maps are made using Thematic Mapper (TM)/Landsat 5 images with spatial resolution of 30 m. The classification accuracy assessment is based on the visual identification of classes using High Resolution Geometric (HRG)/SPOT-5 images at 2.5 m, which are overlapped and compared to the

maps produced by TerraClass. More information about the validation can be obtained in Almeida et al. (2016).

To obtain land cover information for the two ASTER scenes (6/16/2004 and 7/5/2005) we used the 2004 TerraClass map resampled to 15 m resolution to match the ASTER data. We superposed it over the ASTER scenes and visually classified seven classes (primary tropical forest (PF), secondary succession forest (SF), pasture (PA), agriculture (AG), other uses (OU), and waterbodies (WB)). A land cover change map was generated from the difference between the two dates. It was then possible to obtain all the areas covered by PF on 6/16/2004 that were logged at some point after this date and represented PA, AG or SF on 7/5/2005.

To assess the temporal variations of the surface energy and water fluxes over the main terrestrial ecosystems in the study area we selected 24 plots of 12 pixels (15 m), totaling 288 pixels, or ~0.065 km^2, for each class (PF, SF, PA, and AG). To examine the effects of land cover changes we selected: 16 plots of 8 pixels (15 m) for the conversions from PF to PA and PF to SF (totaling 128 pixels, or ~0.029 km^2), and 6 plots of 8 pixels (15 m) for the conversion from PF to AG (totaling 48 pixels, or ~0.01 km^2). A paired samples *t*-test analysis was used in order to compare variation among the biophysical variables. In this analysis, a *t*-value was generated and statistical significance for the differences between and within groups was established at the probability level of 0.01.

2.5 Estimation of surface energy and water fluxes

SEBAL (Bastiaanssen et al., 1998a) was developed to estimate the energy available and the energy fluxes at the surface using daily satellite data and minimal field measurements. Input variables are related to T_{air} and Ws during the satellite overpass. SEBAL has been improved since its conception, including new parametrizations for albedo (Liang, 2001) and G (Bastiaanssen, 2000).

LE is computed as a residual term from the energy balance equation at the time of the satellite overpass:

$$LE = Rn - G - H \quad (1)$$

where Rn is net radiation (W m^{-2}), G is the soil heat flux (W m^{-2}) and H is the sensible heat flux (W m^{-2}).

Rn is calculated using surface reflectance and surface temperature from the satellite. Rn is the result of the energy budget between shortwave and longwave radiation at the surface described as:

$$Rn = (1-\alpha_s)K\downarrow + L\downarrow - L\uparrow - (1-\varepsilon_s)L\downarrow \quad (2)$$

where K↓ is incoming shortwave radiation (W m^{-2}), which in SEBAL is estimated using extraterrestrial radiation estimated from astronomical parameters. α_s is surface albedo,

$L\downarrow$ is incoming longwave radiation (W m^{-2}), which is estimated using the Stefan-Boltzmann equation and near-surface air temperature as well as atmospheric emissivity. $L\uparrow$ is outgoing longwave radiation (W m^{-2}), which is also calculated with the Stefan-Boltzmann equation using remotely sensed surface temperature and surface emissivity (ε_s).

G was modeled as a function of Rn and surface properties expressed by normalized difference vegetation index (NDVI), LST and α_s:

$$G = \left[\frac{LST}{\alpha_s} \left(0.0038\alpha_s + 0.0074\alpha_s^{\,2}\right)\left(1 - 0.98NDVI^4\right) \right] Rn \quad (3)$$

H is calculated by the bulk aerodynamic resistance equation, which uses aerodynamic temperature and aerodynamic resistance to heat transfer (r_{ah}):

$$H = \frac{\rho C_p dT}{r_{ah}} \quad (4)$$

where ρ is air density (kg m^{-3}), C_p is the specific heat of dry air (1004 J kg^{-1} K^{-1}), dT is the air temperature difference (K) between two heights (typically 0.1 m and 2 m), and r_{ah} is the aerodynamic resistance (s m^{-1}) to heat transfer from the land surface to the height of wind speed measurement.

The temperature difference (dT) is estimated at two anchor-pixels, assuming that dT between those pixels is a linear function expressed by:

$$dT = b + aLST \quad (5)$$

where a and b are empirically determined constants.

The determination of a and b involves identifying hot and cold pixels, where it is assumed that the available surface energy is majorly partitioned to H and LE respectively. These pixels are usually selected over bare soil and waterbodies respectively. Once the hot and cold anchor-pixels have been identified, Equation 1 is solved for each pixel in an iterative process that is performed until the r_{ah} term in Equation 4 reaches stability.

The last step of SEBAL is computing daily ET (ET_{24h}) from the evaporative fraction (EF):

$$EF = \frac{LE}{Rn - G} \quad (6)$$

$$ET_{24h} = 86400 \frac{Rn_{24h} EF}{\lambda} \quad (7)$$

where Rn_{24h} is the daily net radiation and λ corresponds to the latent heat of water vaporization. We note that in this study the analyzes are focused on the instantaneous estimates for albedo, Rn, G, H, EF (~10:30 a.m.), and daily estimates for ET.

SEBAL has been applied and validated in different regions (Paiva et al., 2011; Bhattarai et al., 2012; Tang et al., 2013; Yang et al., 2015). The model is sensitive to land cover, allowing analysis in agricultural areas, deserts, prairies, and forests (Senay et al., 2007; Schuurmans et al., 2011). Regarding the accuracy of the estimates, studies indicate relative errors ranging between ~5-17% (Bastiaanssen et al., 1998b; Hemakumara et al., 2003; Kimura et al., 2007; Bhattarai et al., 2012). The primary sources of uncertainty in SEBAL are related to the determination of H and the low sensitivity of the model to soil moisture and water stress. Further details of SEBAL can be found in Bhattarai et al. (2016) and Santos et al. (2017).

2.6 Validation

The estimates of the surface energy and water fluxes obtained from SEBAL and the ASTER data were compared with LBA flux tower observations. The estimated values were extracted from a 67 by 67 pixels (~1 x 1 km^2) window centered on the JBR flux tower. This window was defined considering the fetch of the JBR flux tower which is on the order of 1 km in all directions, as described in von Randow et al. (2004). Two

indices, including bias (Equation 8) and relative error (RE) (Equation 9) were used to assess the accuracy of the estimates:

$$\text{bias} = X_{mod} - X_{obs} \quad (8)$$

$$RE = 100\left|\frac{X_{mod} - X_{obs}}{X_{obs}}\right| \quad (9)$$

where X_{obs} is the flux tower observation and X_{mod} is the modelled value. These indices are commonly used for comparing pairs of variables and allow evaluating the error of data.

3. Results and discussion

3.1 Validation of SEBAL estimates

The mean errors in Rn and ET were approximately 2% and 15% of the field measurements (Table 2). There was an underestimation of -9 and -11 W m^{-2} in Rn and an overestimation of 0.48 and 0.46 mm day^{-1} in ET for the scenes of 6/16/2004 and 7/5/2005, respectively. Studies using SEBAL have been conducted in the Amazon region, such as in Santos et al. (2011), de Oliveira and Moraes (2013), Ferreira et al.

(2013), and de Oliveira et al. (2016). These studies were performed in the southwestern and eastern parts of the Amazon using LBA data from different sites. Input data were acquired from the MODIS and TM sensors. Previous results found relative errors of ~1-16% for Rn and ~25% for ET.

The mean errors in albedo and H were on the order of 15% and 10%, respectively. Albedo tended to be overestimated, with biases varying between 0.016 and 0.018, while H tended to be underestimated, with biases ranging from -5 and -10 W m^{-2}. By way of comparison, Santos et al. (2011) and de Oliveira and Moraes (2013) estimating albedo from TM/Landsat 5 and MODIS/Terra images in Amazonia found errors varying from 0-39% and 13-19%, respectively. The errors obtained for H varied from 8% to 11% and are comparable with other studies (Ma et al., 2002; Timmermans et al., 2007). Recall that the main sources of uncertainties in SEBAL are related to the estimation of this variable (Allen et al., 2011), which requires the determination of the hot and cold pixels. According to Bastiaanssen et al. (1998b), the model also presents a low sensivity to soil moisture and water stress, which especially causes inaccuracies on the estimation of ET either on an instantaneous or daily basis. G was not validated due to the absence of measurements for the study period. Intensive campaigns at the JBR site have shown that G represents ~3% of Rn (Alvala et al., 2002). In our study, G correspondend on average to ~7% of Rn on an instantaneous basis (~10:30 a.m.).

(Table 2)

3.2 Land-cover patterns

The study area is dominated by primary tropical forests (Figure 2; Table 3). Owing to deforestation, it is possible to observe extensive patches of different land cover types such as secondary forests, pastures and croplands (primarily soybeans with coffee and palm oil). Approximately 77% of the study region is covered by forests (primary and secondary). Pastures and agricultural areas occupy ~21% of the region. The remaining of the study region is represented by waterbodies, with the Ji-Parana river as the most representative in terms of total area, and other uses such as bare soils, rocky outcrops and mining.

Rondonia is located within the arc of deforestation, where there is a higher pressure from human settlement (Lambin et al., 2003; Almeida et al., 2016), especially on the western and northeastern sides of the Ji-Parana river where the fish bone pattern of deforestation is observed (Brown et al., 2004). On the western side of the river the rainforest has been progressively cleared during the last 35 years. Most of the area along the eastern flank of the Ji-Parana river is inside the JBR. Altough this area is protected by IBAMA, it has been suffering some small scale slash and burn activities, especially close to the northeastern border (black arrows on Figure 2). However, the disturbed areas inside the JBR are considered small when compared to the extensive areas of pristine forest (von Randow et al., 2004).

Pastures increased 15.5 km^2 (~9%) while agricultural areas decreased 5.9 km^2 (~40%) between 6/16/2004 and 7/5/2005. We note that economic factors may explain

this pattern, since it is common for croplands to rotate with pasture, especially when grain prices are low (Morton et al., 2006; Alves et al., 2009). For this reason, some authors divide croplands between permanent and temporary when studying land cover in Amazonia (Aguiar et al., 2007; Espindola et al., 2012). It was not possible to adopt this division in our mapping due to the limited temporal coverage of the study. Over this 1-year period, there were reductions of 9.6 km^2 (~2%) and 2.8 km^2 (~4%) in the area covered by primary and secondary forests, respectively. From the land cover change data, we observed that of the ~9.6 km^2 logged at some point after 6/16/2004, a total of ~8.9 km^2 (93%) were converted either to pasture (~4.2 km^2), secondary succession forest (~3.6 km^2) or agriculture (~1.1 km^2). The remaining, approximately 0.7 km^2 (7%), were classified in 7/5/2005 either as other uses or water (we note that this case is most likely related to forested areas mapped in the scene of 2004 that were flooded in the scene of 2005).

(Figure 2)

(Table 3)

3.3 Spatio-temporal variations of surface energy and water fluxes over the study area

Figure 3 illustrates the spatial distribution of albedo, Rn, G, H, ET, and EF in the study area on 6/16/2004 and 7/5/2005. The average values between both scenes are

similar. This behavior was not surprising given the fact that the scenes were acquired in the same period of the dry season (June/July), which implies that the land surface was subjected to comparable external environmental conditions (i.e., solar zenith angle). It was observed that the daily average (7 a.m. to 5 p.m.) albedo, G, H, ET, and EF were ~2% (0.144-0.147), ~21% (42-51 W m^{-2}), ~11% (70-78 W m^{-2}), ~2% (3.47-3.59 mm day^{-1}), and ~1% (0.82-0.83) higher in 7/5/2005 in comparison with 6/16/2004. Rn showed a small reduction, on the order of ~1% (525-518 W m^{-2}). This behavior can be understood when analyzing ancillary weather data obtained by the JBR flux tower, such as K↓, T_{air} and PPT (Figure 4). Daily average (7 a.m. to 5 p.m.) K↓ and T_{air} were ~11% and ~25% higher in 7/5/2005 (545 W m^{-2} and 30ºC) in comparison with 6/16/2004 (491 W m^{-2} and 24ºC). Significant differences were observed in accumulated PPT over the 30 days prior to the scenes acquisition. Between 5/17/2004-6/15/2004 and 6/5/2005-7/4/2005 the accumulated PPT corresponded to 51.2 mm and 4.6 mm, respectively. In 2005, the Amazon basin experienced one of most intense drought episodes of the last 100 years (Marengo et al., 2008; Zeng et al., 2008).

G and H are proportional to the K↓ and T_{air}, and local studies in Amazonia have shown that the highest albedo values and, consequently, the lowest Rn values generally occur at the same time as the driest soil moisture conditions (Gash and Nobre, 1997; von Randow et al., 2004). Thus, the increase in G, H and albedo, and decrease in Rn in the 2005 scene were predictable. Regarding ET, a higher average value would be expected in the 2004 scene especially given the greater availability of moisture at the

surface. However, it was observed that ET was higher in the 2005 scene. It is important to note here that the averages for the whole scene level are not statistically significant.

According to previous literature, there is no clear pattern regarding the increase or decrease of ET over the Amazon rainforests during seasonal water deficits. Recent work has shown a pattern of increased ET during dry periods in Amazonia (Hutyra et al., 2007; de Oliveira et al., 2017; Maeda et al., 2017). This is due to (1) the ability of the Amazonian tree species to draw water from deeper soils, accessing water stored even from past rainy periods, and (2) increases in solar radiation at the surface, due to decreased cloud cover. On the other hand, other studies have shown a pattern of higher ET under moist conditions than under dry conditions in Amazonia (Malhi et al., 2002; Sommer et al., 2002; Borma et al., 2009). These studies attribute this behavior to (1) regional differences in forest structure, (2) longer dry seasons, (3) lower annual rainfall rates, and (4) lower moisture stored in the soil. Recall that most of the study area is comprised of primary forests. Our results suggest that ET over forests in this part of Amazonia may not be water limited even when experiencing drought conditions. We hypothesize that in this region, the interaction between solar radiation, canopy physiology (i.e., quantity and age of leaves) and its ecohydrological mechanisms (i.e., root networks which exploit soil water), is more important than water availability. This interaction has an effect in the stomatal resistance to transpiration, which factors the partitioning of Rn into sensible, soil and latent heat (Christoffersen et al., 2014; Albert et al., 2018).

Analyzing Figures 2 and 3 helps to understand the variability of the surface fluxes according to the land cover in the region. It is possible to verify the difference in albedo between logged and forested areas, with the latter presenting lower values. Because they are darker, forests have a lower albedo and therefore absorb more solar radiation than short vegetation (Culf et al., 1995; Priante-Filho et al., 2004). The highest values of Rn are in the eastern part of the study area, which has experienced less deforestation compared to the western region. Rn over forest areas is higher than in pasture or agricultural areas due to differences in the absorbed solar radiation and longwave radiation balance (Bastable et al., 1993; Davidson et al., 2012). The deforested areas have the highest amounts of sensible heat. Clear-cutting of mature forests tends to increase LST and alter the emissivity, resulting in an increase in incoming/outgoing longwave radiation (Souza Filho et al., 2006; Aguiar et al., 2011). ET and EF over forested areas was higher than non-forested areas. This difference in ET and EF between these areas is related to variation in plant structure and physiology, which in turn causes differences in their water use (Zhang et al., 2014; Yang et al., 2016). The highest values of ET and EF are located in the eastern portion of the study area, which occurred as expected since this region is better preserved in terms of deforestation.

(Figure 3)

(Figure 4)

3.4 Surface energy and water fluxes for different land cover types

The aforementioned results illustrate that changes in energy and water cycling in the study area are a function of land cover (Song et al. 2015; Khanna et al., 2017). Now a more comprehensive analysis can be conducted concerning the dynamics of albedo, Rn, G, H, ET, and EF over different ecosystems in the study area. Figure 5 illustrates some of the plots used to extract the SEBAL estimates for each one of the different land cover types (PF, SF, PA, and AG) and Figure 6 shows the magnitudes of the surface fluxes for 6/16/2004 and 7/5/2005. The natural ecosystems (PF and SF) presented higher Rn, ET and EF, and lower albedo, G and H than the anthropic ecosystems (PA and AG). A small fluctuation of albedo values (from ~1% to 5%) was observed between the two scenes in the different ecosystems. The average albedo ranged from 0.135 (PF) to 0.20 (AG), illustrating a difference of ~48%. SF showed an average albedo of 0.158, while PA had a value of 0.190. These results indicate that PF and SF have, on average, an albedo ~19% lower than AG and PA ($p<0.01$, *t*-value=26.66, n=576). Studies conducted over forest, pasture, and soybean crops in Amazonia have shown values of about 0.134, 0.18 and 0.20, which are comparable to those obtained here (Shuttleworth, 1989; Culf et al., 1995; Souza et al., 2010).

All land cover types had higher values of Rn in 6/16/2004 than in 7/5/2005. It follows the pattern observed for the whole study area, as discussed in section 3.3. Rn over AG varied between 478 W m^{-2} (6/16/2004) and 468 W m^{-2} (7/5/2005) (mean=473

W m^{-2}) while Rn over PA varied between 487 W m^{-2} (6/16/2004) and 480 W m^{-2} (7/5/2005) (mean=483 W m^{-2}). This is a difference of ~2% in Rn between both ecosystems ($p<0.01$, *t*-value=12.92, n=288). Wright et al. (1992) and Galvao and Fisch (2000) observed for pasture sites in Amazonia values about 500 W m^{-2} at ~10:30 a.m. In the forest areas (SF and PF), we found values ranging between 517 and 543 W m^{-2} on 6/16/2004 and between 513 and 533 W m^{-2} for 7/5/2005. SF had a mean value of 515 W m^{-2}, while PF had a value of 538 W m^{-2}. It is possible to observe that Rn over forested areas is ~10% greater in comparison with agricultural and pasture lands ($p<0.01$, *t*-value=23.69, n=576). Analyzes by von Randow et al. (2004) and Aguiar et al. (2006) observed values of 450 and 530 W m^{-2} over forest sites in the southwestern part of Amazonia (~10:30 a.m.).

Our results for G showed that AG had, on average, the highest values (96 W m^{-2}), followed by PA (92 W m^{-2}), SF (57 W m^{-2}) and PF (32 W m^{-2}). A similar behavior was found for H (AG=293 W m^{-2}, PA=247 W m^{-2}, SF=113 W m^{-2}, and PF=36 W m^{-2}). G was larger over the four land cover types in 2005 when compared to 2004. Higher increases were observed for AG (90 to 103 W m^{-2}) and PA (86 to 98 W m^{-2}) (both ~14%) while lower increases were observed for PF (31 to 34 W m^{-2}) (~10%) and SF (55 to 58 W m^{-2}) (~5%). H was larger over AG and PA in the scene from 2005 in comparison with 2004 (~1% and ~2%), but PF and SF reduced it rates (~10% and 15%). This behavior can be understood when analyzing EF over the different ecosystems. EF over PF and SF was ~1% and ~4% greater in 2005 than in 2004 (0.92 to 0.93 and 0.74 to 0.77, respectively). For AG and PA, EF decreased in 2005 compared to 2004 in

~24% (0.25 to 0.19) and 10% (0.34 to 0.39), respectively. Recall that 2005 was a drought year therefore the land surface was subjected to drier conditions than in 2004. The mechanisms of interaction between solar radiation and canopy physiology, which is dependent both by the plant (i.e., stomatal conductance and the root networks which exploit soil water) and environmental conditions (i.e., T_{air} and vapor pressure deficit), are most likely to have a greater impact than water availability in ET over forests in this part of Amazonia (Rocha et al., 2004; Christoffersen et al., 2014; de Oliveira et al., 2017; Albert et al., 2018). Therefore, we suggest that this lack of response to moisture availability is related to both the control of canopy stomatal conductance on vegetation water use and the deeper roots of Amazonian tree species, which allows access to deeper water (Malhi et al., 2002; Saleska et al., 2007). These results make evident that the water limitation in this part of Amazonia tends to affect the anthropic ecosystems (AG and PA) more than the natural ones (PF and SF). This is related to the vegetative structure, photosynthetic capacity and different physiological mechanisms among these ecosystems.

The higher EF over PF and SF on 7/5/2005 compared to 6/16/2004 caused an increase in ET over these ecosystems of ~7% (3.88 to 4.15 mm day^{-1}) and ~1% (3.22 to 3.26 mm day^{-1}), respectively. It is interesting to note that the ET increase was ~6% higher in the primary forests to that observed for the secondary forest areas. This behavior may be related to specific soil-land-atmosphere conditions in the dates analyzed as well as the physiological needs of the plants, depending on their development stage. It is important to note that in the early forest stages the ET rates are

low but as the forest approaches maturity the ET rates increase markedly (Holscher et al., 1997; Giambelluca, 2002). As expected, due to the decrease in EF over AG and PA on 7/5/2005 compared to 6/16/2004, these ecosystems presented reductions in ET rates on the order of ~17% (0.92 to 0.76 mm day^{-1}) and 3% (1.45 to 1.40 mm day^{-1}), respectively. Taking into consideration the average between the two dates, it was observed that the ET values among the four ecosystems ranged from 0.84 mm day^{-1} (AG) to 4.01 mm day^{-1} (PF). PA and SF showed intermediate values near 1.43 mm day^{-1} and 3.24 mm day^{-1}, respectively. By way of comparison, local studies developed in different parts of Amazonia showed ET values during the dry season varying from 3.4-4.0 mm day^{-1} for forests (Rocha et al., 2004; von Randow et al., 2004) and from 1.93-2.73 mm day^{-1} for pasture/annual crops (Galvao and Fisch 2000; Webler et al., 2013), which are comparable to those found here.

(Figure 5)

(Figure 6)

3.5 Effects of land-cover changes

Three situations were selected to analyze the effects of land cover changes in Amazonia on the surface energy and water fluxes: (1) PF to PA, (2) PF to AG and (3) PF to SF. Table 4 and Figure 7 present the absolute and relative values of albedo, Rn, G,

H, ET, and EF for each scenario of land cover change. The conversion of primary forests to pasture, agricultural and secondary succession areas caused an increase in albedo, G and H, and a decrease in Rn, ET and EF. The increase in albedo is mainly related to the fact that the leaves from grasslands, croplands and secondary forests reflect more and absorb less solar radiation than primary forests. The increases observed in G and H are most likely related to the higher surface and air temperatures observed over areas with low vegetation coverage. The decrease in Rn is related to the increase in albedo and LST, while the decreases in ET and EF occurred due to the lower surface aerodynamic roughness, lower leaf area, and shallower rooting depth of pastures, croplands and secondary forests compared to primary forests. Our results are in agreement with several studies conducted in the Amazon region involving the impact of the deforestation on land-atmosphere exchanges based on micrometeorological experiments and regional earth system modeling (Nobre et al., 1991; Henderson-Sellers et al., 1993; Costa and Foley, 1999; Moraes et al., 2004; Sampaio et al., 2007; Panday et al., 2015; Khanna et al., 2017; Guimberteau et al., 2017).

In situations 1 (PF to PA) and 2 (PF to AG), the largest relative impact was observed for H (53 to 178 W m^{-2} (~236%) and 55 to 195 W m^{-2} (~255%)) while the smallest was observed for Rn (539 to 504 W m^{-2} (~6%) and 535 to 495 W m^{-2} (~7%)). Sampaio et al. (2007) found that the conversion from primary forests to pasture in Amazonia caused an increase in H and Rn of ~43% and 6%, respectively. For the conversion from primary forests to soybean cropland the authors found increases of ~54% in H and ~7% in Rn. Here, the impact on H is higher but the effects on Rn are

similar to those found in Sampaio's et al. study. The effects related to the conversion from PF to PA on Rn are comparable to those described by Lean et al. (1996), which showed a decrease of ~9%. In the primary forest areas before the conversion to PA and AG, it is observed that G and H consume ~7% and ~10% of Rn. After the conversion to PA, it is noted that G and H consume ~18% and ~35% of Rn. Following the conversion to AG, G and H corresponded to ~19% and ~39% of Rn. These results show that the deforestation and consequent transition to pasture or soybean increases approximately two to four times the total energy used to heat the soil subsurface (G) (34 to 93 W m^{-2}) ($p<0.01$, *t*-value=32.29, n=176) and raises the T_{air} (H) (54 to 187 W m^{-2}) ($p<0.01$, *t*-value=56.15, n=176), respectively.

The albedo values increased ~20% (0.136-0.163) ($p<0.01$, *t*-value=8.45, n=128) in the conversion from PF to PA and ~23% (0.141-173) ($p<0.01$, *t*-value=7.48, n=48) in the conversion from PF to AG. Bastable et al. (1993) and Costa et al. (2007) reported increases of ~24% (0.131-0.163) and ~62% (0.125-0.205) for pastureland and soybean deforestation scenarios. EF decreased approximately 36% and 43% for situations 1 ($p<0.01$, *t*-value=102.21, n=128) and 2 ($p<0.01$, *t*-value=219.72, n=48), respectively. The EF values changed from 0.89-0.57 (PF to PA) and 0.89-0.51 (PF to AG). von Randow et al. (2004) reported EF values for the conversion from primary forest to pasture from 0.74-0.56, showing a decrease of ~24%. EF values related to the change from primary forest to agricultural areas in Amazonia were not found in the literature. As expected, EF decreased in similar relative rates to those found for ET. It was observed that the conversion from PF to PA reduced ET in ~35% (~1.30 mm day^{-1})

($p<0.01$, *t*-value=39.78, n=128) while the conversion from PF to AG reduced ET in ~42% (~1.54 mm day^{-1}) ($p<0.01$, *t*-value=42.09, n=48). Sampaio et al. (2007) investigating cases of deforestation in Amazonia reported reductions of ~26% (~1.0 mm day^{-1}) for the conversion to pasture and ~31% (~1.2 mm day^{-1}) for the conversion to soybean.

Situation 3 illustrates a common scenario in the Amazon region, which is the development of SF in areas of abandoned clearcuts, abandoned pasture and abandoned mechanized fields. Considering the time interval between the two scenes (~1-year), it is most likely that the secondary succession areas analyzed are related to the abandonment immediately after clearcuts of mature forest (that is, after logging the land was not used for cattle or extensive agriculture). The relative variations in albedo and Rn were comparable to the ones observed for the scenarios of conversion from PF to PA and PF to AG. The most considerable effects on the surface fluxes occurred in G (29 to 64 W m^{-2}, or a mean increase of ~119%) ($p<0.01$, *t*-value=13.95, n=128) and H (47 to 95 W m^{-2}, or a mean increase of ~103%) ($p<0.01$, *t*-value=8.81, n=128). The values of G and H observed for situation 3 were ~17% and ~43% lower than those observed for situation 1 and ~56% and ~60% lower in comparison with situation 2. The conversion of PF to SF incurred in reductions on EF of ~13% (~0.91-0.79) ($p<0.01$, *t*-value=9.38, n=128) and on ET of 12% (~3.92-3.43 mm day^{-1}) ($p<0.01$, *t*-value=8.36, n=128). It is interesting to note that the decrease in ET was ~0.49 mm day^{-1}, which is ~62% and 68% lower than the reductions observed in ET for situations 1 and 2. To date, limited research has been conducted to understand the coupling between secondary forests and

the atmosphere over the Amazon region. We highlight that the results obtained here are in agreement with these studies, which have shown that evaporation accounts for ~80% of Rn over young secondary vegetation in comparison with 90% for primary forest evaporation (Holscher et al., 1997; Giambelluca et al., 1997; Jipp et al., 1998; Giambelluca et al., 2000; Giambelluca, 2002; Feldpausch et al., 2005). An interesting aspect is that some of these studies reported recovery of ET within 15 years to values for primary forest. The recovery of high ET rates may have implications for the regional climate, since ~25-56% of the Amazon basin rainfall is derived from recycling water evaporated within the basin (Eltahir and Bras, 1996; Feldpausch et al., 2005).

Summarizing the combined effects on the surface energy and water fluxes between undisturbed natural forest ecosystems (PF) and disturbed areas (PA, AG and SF) in the region, our results demonstrate that albedo, G and H tend to increase 23%, 157% and 19% whilst Rn, ET and EF tend to decrease 7%, 30% and 31%, respectively.

(Figure 7)

(Table 4)

4. Concluding remarks

In this study, ASTER images and LBA field observations were used to examine the partitioning of surface energy and water fluxes over different land cover types in one

wet year (2004) and one drought year (2005) in a fragmented region of the arc of deforestation in Brazil. The SWIR (30 m) and TIR (90 m) bands were resampled to the 15 m of the VNIR bands, making this study the first to examine the land-atmosphere interactions in Amazonia with such high spatial resolution. Comparison between estimates obtained by SEBAL and measurements collected at JBR flux tower showed errors of 2% for instantaneous Rn and 13% for daily ET. The spatial variation of albedo, Rn, G, H, ET, and EF were mainly related to the lower presence of forest (primary or secondary) in the western side of the Ji-Parana river in comparison with the eastern side, which is inside of the JBR protected area. It was noted that drought events and, consequently, water limitation in this part of Amazonia tend to affect the ecosystems considered anthropic (AG and PA) more than those considered natural (PF and SF). This is related to the fact that due to the deep roots, Amazonian tree species have an ability to draw water from deeper soil layers, thus accessing water stored from past rainy periods.

We found statistically significant differences on the surface energy and water fluxes prior to and ~1-year after the deforestation. It was observed that Rn over forested areas (~527 W m^{-2}) is ~10% greater in comparison with agricultural and pasture lands (~478 W m^{-2}). In addition, we observed that the deforestation and consequent transition to pastures or croplands increase in two to four times the total energy used to heat the soil subsurface (G) and raises the T_{air} (H). These differences in energy partitioning contribute to approximately three times higher ET over forested areas (~408 W m^{-2}, or 3.63 mm day^{-1}) in comparison with non-forested areas (~114 W m^{-2}, or 1.14 mm day^{-1}).

Factors such as variation in plant structure and physiology and moisture availability cause these differences in the absorption/reflection of solar radiation and water losses. The conversion of PF to AG is likely to have a higher impact on the local climate in this part of Amazonia when compared to the change to PA and SF, due to the fact that the conversion of PF to AG implies a lower Rn and ET and higher G and H. Less impact occurred in the surface energy and water fluxes with the modification to SF. Considering the fact that the secondary forests analyzed here are only ~1-year old and as they approach maturity the ET rates tend increase markedly, these results illustrate the importance of conserving secondary forest areas in Amazonia. We conclude that our methodology based on the use of high-resolution satellite data was a useful proposition to analyze the local surface energy and water exchanges in southwestern Amazonia. The information obtained may be used as inputs in earth system surface models allowing to evaluate the impact, both at regional and global scales, caused by land cover changes.

Acknowledgements

Gabriel de Oliveira acknowledges CNPq (Grant No. 52521/2012-7) and CAPES (Grant No. 8210/2014-4) agencies for providing research fellowships. We thank the LBA Rondonia Regional Office for providing the flux tower data for this work.

References

Abrams, M., Tsu, H., Hulley, G., Iwao, K., Pieri, D., Cudahy, T., Kargel, J., 2015. The advanced spaceborne thermal emission and reflection radiometer (ASTER) after fifteen years: review of global products. International Journal of Applied Earth Observation and Geoinformation. 38, 292-301.

Aguiar, A.P.D., Câmara, G., Escada, M.I.S., 2007. Spatial statistical analysis of land-use determinants in the Brazilian Amazonia: exploring intra-regional heterogeneity. Ecological Modelling. 209, 169-188.

Aguiar, L.J.G., Costa, J.M.N.D., Fisch, G.R., Aguiar, R.G., Costa, A.C.L.D., Ferreira, W.P.M., 2011. Estimate of the atmospheric longwave radiation in forest and pasture areas in southwest Amazon. Brazilian Journal of Meteorology. 2, 211-224.

Aguiar, R.G., Manzi, A.O., Priante Filho, N., Sá, L.D., Cardoso, F.L., von Randow, C., 2006. Mass and energy flux over tropical forest in the southwest Amazon. Brazilian Journal of Meteorology. 21, 248-257.

Albert, L.P., Wu, J., Prohaska, N., Camargo, P.B., Huxman, T.E., Tribuzy, E.S., Ivanov, V.Y., Oliveira, R.S., Garcia, S., Smith, M.N., Oliveira Junior, R.C., 2018. Age - dependent leaf physiology and consequences for crown -scale carbon up dry season in an Amazon evergreen forest. New Phytologist. 218, 1-15.

Allen, R., Irmak, A., Trezza, R., Hendrickx, J.M., Bastiaanssen, W., Kjaersgaard, J., 2011. Satellite Based and ET estimation

METRIC. Hydrological Processes. 25, 4011-4027.

Almeida, C.A.D., Coutinho, A.C., Esquerdo, J.C.D.M., Adami, M., Venturieri, A., Diniz, C.G., Dessay, N., Durieux, L., Gomes, A.R., 2016. High spatial resolution land use and land cover mapping of the Brazilian Legal Amazon in 2008 using Landsat-5/TM and MODIS data. Acta Amazonica. 46, 291-302.

Alvalá, R.D.S., Gielow, R., Da Rocha, H.R., Freitas, H.C., Lopes, J.M., Manzi, A.O., Von Randow, C., Dias, M.S., Cabral, O.M.R., Waterloo, M.J., 2002. Intradiurnal and seasonal variability of soil temperature, heat flux, soil moisture content, and thermal properties under forest and pasture in Rondonia. Journal of Geophysical Research: Atmospheres. 107, 1-10.

Alves, D.S., Morton, D.C., Batistella, M., Roberts, D.A., Souza Jr., C., 2009. The changing rates and patterns of deforestation and land use in Brazilian Amazonia. In: Keller, M., Bustamante, M., Gash, Dias, P.S., Jr. (Eds.). Amazonia and Global Change (11-23). Washington: AGU.

Andreae, M.O., Artaxo, P., Brandao, C., Carswell, F.E., Ciccioli, P., Costa, A.L., Culf, A.D., Esteves, J.L., Gash, J.H.C., Grace, J., Kabat, P., 2002. Biogeochemical cycling of

carbon, water, energy, trace gases, and aerosols in Amazonia: the LBA -EUSTACH experiments. Journal of Geophysical Research: Atmospheres. 107, 1-33.

Aragao, L.E., Poulter, B., Barlow, J.B., Anderson, L.O., Malhi, Y., Saatchi, S., Phillips, O.L., Gloor, E., 2014. Environmental change and the carbon balance of Amazonian forests. Biological Reviews. 89, 913-931.

Bastable, H.G., Shuttleworth, W.J., Dallarosa, R.L.G., Fisch, G., Nobre, C.A., 1993. Observations of climate, albedo, and surface radiation over cleared and undisturbed Amazonian forest. International Journal of Climatology. 13, 783-796.

Bastiaanssen, W.G., Menenti, M., Feddes, R.A., Holtslag, A.A.M., 1998a. A remote sensing surface energy balance algorithm for land (SEBAL). 1. Formulation. Journal of Hydrology. 212, 198-212.

Bastiaanssen, W.G.M., 2000. SEBAL-based sensible and latent heat fluxes in the irrigated Gediz Basin, Turkey. Journal of Hydrology. 229, 87-100.

Bastiaanssen, W.G.M., Pelgrum, H., Wang, J., Ma, Y., Moreno, J.F., Roerink, G.J., Van der Wal, T., 1998b. A remote sensing surface energy balance algorithm for land (SEBAL).: Part 2: Validation. Journal of Hydrology. 212, 213-229.

Bhattarai, N., Dougherty, M., Marzen, L.J. and Kalin, L., 2012. Validation of evaporation estimates from a modified surface energy balance algorithm for land (SEBAL) model in the south-eastern United States. Remote Sensing Letters. 3, 511-519.

Bhattarai, N., Shaw, S.B., Quackenbush, L.J., Im, J., Niraula, R., 2016. Evaluating five remote sensing based single-source surface energy balance models for estimating daily evapotranspiration in a humid subtropical climate. International Journal of Applied Earth Observation and Geoinformation. 49, 75-86.

Bonan, G.B., 2008. Forests and climate change: forcings, feedbacks, and the climate benefits of forests. Science. 320, 1444-1449.

Borma, L.D.S., Da Rocha, H.R., Cabral, O.M., Von Randow, C., Collicchio, E., Kurzatkowski, D., Brugger, P.J., Freitas, H., Tannus, R., Oliveira, L., Rennó, C.D., 2009. Atmosphere and hydrological controls of the evapotranspiration over a floodplain forest in the Bananal Island region, Amazonia. Journal of Geophysical Research: Biogeosciences. 114, 1-12

Broedel, E., Tomasella, J., Cândido, L.A., Randow, C., 2017. Deep soil water dynamics in an undisturbed primary forest in central Amazonia: differences between normal years and the 2005 drought. Hydrological Processes. 31, 1749-1759.

Brown, J.C., Jepson, W., Price, K.P., 2004. Expansion of mechanized agriculture and land-cover change in southern Rondonia, Brazil. Journal of Latin American Geography. 3, 96-102.

Butt, N., De Oliveira, P.A., Costa, M.H., 2011. Evidence that deforestation affects the onset of the rainy season in Rondonia, Brazil. Journal of Geophysical Research: Atmospheres. 116, 1-8.

Christoffersen, B.O., Restrepo-Coupe, N., Arain, M.A., Baker, I.T., Cestaro, B.P., Ciais, P., Fisher, J.B., Galbraith, D., Guan, X., Gulden, L., van den Hurk, B., 2014. Mechanisms of water supply and vegetation demand govern the seasonality and magnitude of evapotranspiration in Amazonia and Cerrado. Agricultural and Forest Meteorology. 191, 33-50.

Costa, M.H., Foley, J.A., 1999. Trends in the hydrologic cycle of the Amazon basin. Journal of Geophysical Research: Atmospheres. 104, 14189-14198.

Costa, M.H., Yanagi, S.N., Souza, P.J., Ribeiro, A., Rocha, E.J., 2007. Climate change in Amazonia caused by soybean cropland expansion, as compared to caused by pastureland expansion. Geophysical Research Letters. 34, 1-4.

Culf, A.D., Fisch, G., Hodnett, M.G., 1995. The albedo of Amazonian forest and ranch land. Journal of Climate. 8, 1544-1554.

Davidson, E.A., de Araújo, A.C., Artaxo, P., Balch, J.K., Brown, I.F., Bustamante, M.M., Coe, M.T., DeFries, R.S., Keller, M., Longo, M., Munger, J.W., 2012. The Amazon basin in transition. Nature. 481, 321-328.

de Oliveira, G., Brunsell, N.A., Moraes, E.C., Bertani, G., dos Santos, T.V., Shimabukuro, Y.E., Aragao, L.E., 2016. Use of MODIS sensor images combined with reanalysis products to retrieve net radiation in Amazonia. Sensors. 16, 91-28.

de Oliveira, G., Brunsell, N.A., Moraes, E.C., Shimabukuro, Y.E., Bertani, G., dos Santos, T.V., Aragao, L.E., 2017. Evaluation of MODIS-based estimates of water-use efficiency in Amazonia. International Journal of Remote Sensing. 38, 5291-5309.

de Oliveira, G., Moraes, E. C., 2013. Validation of net radiation obtained through MODIS/TERRA data in Amazonia with LBA surface measurements. Acta Amazonica. 3, 353-364.

El-Masri, B., Barman, R., Meiyappan, P., Song, Y., Liang, M., Jain, A.K., 2013. Carbon dynamics in the Amazonian Basin: integration of eddy covariance and ecophysiological data with a land surface model. Agricultural and Forest Meteorology. 182, 156-167.

Eltahir, E.A., Bras, R.L., 1996. Precipitation recycling. Reviews of Geophysics. 34, 367-378.

Espindola, G.M., De Aguiar, A.P.D., Pebesma, E., Câmara, G., Fonseca, L., 2012. Agricultural land use dynamics in the Brazilian Amazon based on remote sensing and census data. Applied Geography. 32, 240-252.

Feldpausch, T.R., Riha, S.J., Fernandes, E.C., Wandelli, E.V., 2005. Development of forest structure and leaf area in secondary forests regenerating on abandoned pastures in Central Amazonia. Earth Interactions. 9, 1-22.

Ferreira, J., Sousa, A.M., Vitorino, M.I., De Souza, E.B., Souza, P.J.O.P., 2013. Estimate of evapotranspiration in the eastern Amazon using SEBAL. Amazonian Journal of Agricultural and Environmental Sciences. 56, 33-39.

French, A.N., Hunsaker, D.J., Thorp, K.R., 2015. Remote sensing of evapotranspiration over cotton using the TSEB and METRIC energy balance models. Remote Sensing of Environment. 158, 281-294.

French, A.N., Jacob, F., Anderson, M.C., Kustas, W.P., Timmermans, W., Gieske, A., Su, Z., Su, H., McCabe, M.F., Li, F., Prueger, J., 2005. Surface energy fluxes with the

Advanced Spaceborne Thermal Emission and Reflection radiometer (ASTER) at the Iowa 2002 SMACEX site (USA). Remote Sensing of Environment., 99, 55-65.

Frohn, R.C., Hao, Y., 2006. Landscape metric performance in analyzing two decades of deforestation in the Amazon Basin of Rondonia, Brazil. Remote Sensing of Environment. 100, 237-251.

Fuchs, H., Magdon, P., Kleinn, C., Flessa, H., 2009. Estimating aboveground carbon in a catchment of the Siberian forest tundra: combining satellite imagery and field inventory. Remote Sensing of Environment. 113, 518-531.

Fujisada, H., Bailey, G.B., Kelly, G.G., Hara, S., Abrams, M.J., 2005. Aster DEM performance. IEEE transactions on Geoscience and Remote Sensing. 43, 2707-2714.

Galleguillos, M., Jacob, F., Prévot, L., French, A., Lagacherie, P., 2011. Comparison of two temperature differencing methods to estimate daily evapotranspiration over a Mediterranean vineyard watershed from ASTER data. Remote Sensing of Environment. 115, 1326-1340.

Galvão, J.D.C., Fisch, G., 2000. Energy balance in forest and pasture areas in Amazonia (Ji-Parana, RO). Brazilian Journal of Meteorology. 2, 25-37.

Gash, J.H.C., Huntingford, C., Marengo, J.A., Betts, R.A., Cox, P.M., Fisch, G., Fu, R., Gandu, A.W., Harris, P.P., Machado, L.A.T., von Randow, C., 2004. Amazonian climate: results and future research. Theoretical and Applied Climatology. 78, 187-193.

Gash, J.H.C., Nobre, C.A., 1997. Climatic effects of Amazonian deforestation: some results from ABRACOS. Bulletin of the American Meteorological Society. 5, 823-830.

Giambelluca, T.W., 2002. Hydrology of altered tropical forest. Hydrological Processes. 16, 1665-1669.

Giambelluca, T.W., Hölscher, D., Bastos, T.X., Frazão, R.R., Nullet, M.A., Ziegler, A.D., 1997. Observations of albedo and radiation balance over postforest land surfaces in the eastern Amazon Basin. Journal of Climate. 10, 919-928.

Giambelluca, T.W., Nullet, M.A., Ziegler, A.D., Tran, L., 2000. Latent and sensible energy flux over deforested land surfaces in the eastern Amazon and northern Thailand. Singapore Journal of Tropical Geography. 21, 107-130.

Gonçalves, L.G.G., Borak, J.S., Costa, M.H., Saleska, S.R., Baker, I., Restrepo-Coupe, N., Muza, M.N., Poulter, B., Verbeeck, H., Fisher, J.B., Arain, M.A., 2013. Overview of the large-scale biosphere–atmosphere experiment in Amazonia Data Model

Intercomparison Project (LBA-DMIP). Agricultural and Forest meteorology. 182, 111-127.

Gowda, P.H., Chavez, J.L., Colaizzi, P.D., Evett, S.R., Howell, T.A., Tolk, J.A., 2008. ET mapping for agricultural water management: present status and challenges. Irrigation Science. 26, 223-237.

Guimberteau, M., Ciais, P., Ducharne, A., Boisier, J.P., Aguiar, A.P.D., Biemans, H., De Deurwaerder, H., Galbraith, D., Kruijt, B., Langerwisch, F., Poveda, G., 2017. Impacts of future deforestation and climate change on the hydrology of the Amazon Basin: a multi-model analysis with a new set of land-cover change scenarios. Hydrology and Earth System Sciences. 210, 1455-1475.

Hais, M., Kucera, T., 2009. The influence of topography on the forest surface temperature retrieved from Landsat TM, ETM+ and ASTER thermal channels. ISPRS Journal of Photogrammetry and Remote Sensing. 64, 585-591.

Hasler, N., Avissar, R., 2007. What controls evapotranspiration in the Amazon basin?. Journal of Hydrometeorology. 8, 380-395.

Hemakumara, H.M., Chandrapala, L., Moene, A.F., 2003. Evapotranspiration fluxes over mixed vegetation areas measured from large aperture scintillometer. Agricultural Water Management. 58, 109-122.

Henderson-Sellers, A., Dickinson, R.E., Durbidge, T.B., Kennedy, P.J., McGuffie, K., Pitman, A.J., 1993. Tropical deforestation: modeling local-to regional-scale climate change. Journal of Geophysical Research: Atmospheres. 98, 7289-7315.

Hölscher, D., Sá, T.D.A., Bastos, T.X., Denich, M., Fölster, H., 1997. Evaporation from young secondary vegetation in eastern Amazonia. Journal of Hydrology. 193, 293-305.

Hutyra, L.R., Munger, J.W., Saleska, S.R., Gottlieb, E., Daube, B.C., Dunn, A.L., Amaral, D.F., De Camargo, P.B., Wofsy, S.C., 2007. Seasonal controls on the exchange of carbon and water in an Amazonian rain forest. Journal of Geophysical Research: Biogeosciences. 112, 1-16.

Jipp, P.H., Nepstad, D.C., Cassel, D.K., Carvalho, C. R. 1998. Deep soil moisture storage and transpiration in forests and pastures of seasonally-dry Amazonia. Climatic Change. 39, 395-412.

Khand, K., Numata, I., Kjaersgaard, J., Vourlitis, G.L., 2017. Dry Season evapotranspiration dynamics over human-impacted landscapes in the southern Amazon using the Landsat-based METRIC model. Remote Sensing. 9, 1-20.

Khanna, J., Medvigy, D., Fueglistaler, S., Walko, R., 2017. Regional dry-season climate changes due to three decades of Amazonian deforestation. Nature Climate Change. 7, 200-204.

Kimura, R., Bai, L., Fan, J., Takayama, N., Hinokidani, O., 2007. Evapotranspiration estimation over the river basin of the Loess Plateau of China based on remote sensing. Journal of Arid Environments. 68, 53-65.

Lambin, E.F., Geist, H.J., Lepers, E., 2003. Dynamics of land-use and land-cover change in tropical regions. Annual Review of Environment and Resources. 28, 205-241.

Lean, J., Button, C. B., Nobre, C. A., Rowntree, P. R., 1996. The simulated impact of Amazonian deforestation on climate using measured ABRACOS vegetation characteristics. In: Gash, J. H. C., Nobre, C. A., Roberts, J. M., Victoria, R. L. (Eds.). Amazonian Deforestation and Climate (549-576). Chichester: John Wiley & Sons.

Li, Z.L., Tang, R., Wan, Z., Bi, Y., Zhou, C., Tang, B., Yan, G., Zhang, X., 2009. A review of current methodologies for regional evapotranspiration estimation from remotely sensed data. Sensors. 9, 3801-3853.

Liang, S., 2001. Narrowband to broadband conversions of land surface albedo I: Algorithms. Remote Sensing of Environment. 76, 213-238.

Lu, D., Weng, Q., 2006. Spectral mixture analysis of ASTER images for examining the relationship between urban thermal features and biophysical descriptors in Indianapolis, Indiana, USA. Remote Sensing of Environment. 104, 157-167.

Ma, Y., Tsukamoto, O., Ishikawa, H., Su, Z., Menenti, M., Wang, J., Wen, J., 2002. Determination of regional land surface heat flux densities over heterogeneous landscape of HEIFE integrating satellite remote sensing with field observation. Journal of the Meteorological Society of Japan. 80, 485-501.

Maeda, E.E., Ma, X., Wagner, F.H., Kim, H., Oki, T., Eamus, D., Huete, A., 2017. Evapotranspiration seasonality across the Amazon Basin. Earth System Dynamics. 8, 439-454.

Malhi, Y., Pegoraro, E., Nobre, A.D., Pereira, M.G.P., Grace, J., Culf, A.D., Clement, R., 2002. Energy and water dynamics of a central Amazonian rain forest. Journal of Geophysical Research: Atmospheres. 107, 1-45.

Marengo, J.A., Nobre, C.A., Tomasella, J., Oyama, M.D., Sampaio de Oliveira, G., de Oliveira, R., Camargo, H., Alves, L.M., Brown, I.F., 2008. The drought of Amazonia in 2005. Journal of Climate. 21, 495-516.

Moraes, E.C., Franchito, S.H. and Brahmananda Rao, V., 2004. Effects of biomass burning in Amazonia on climate: a numerical experiment with a statistical -dynamical model. Journal of Geophysical Research: Atmospheres. 109, 1-12.

Morton, D.C., DeFries, R.S., Shimabukuro, Y.E., Anderson, L.O., Arai, E., Espirito-Santo, F., Freitas, R., Morisette, J., 2006. Cropland expansion changes deforestation dynamics in the southern Brazilian Amazon. Proceedings of the National Academy of Sciences. 103, 14637-14641.

Nobre, C.A., Sellers, P.J., Shukla, J., 1991. Amazonian deforestation and regional climate change. Journal of Climate. 4, 957-988.

Numata, I., Khand, K., Kjaersgaard, J., Cochrane, M.A., Silva, S.S., 2017. Evaluation of Landsat-based METRIC modeling to provide high-spatial resolution evapotranspiration estimates for Amazonian forests. Remote Sensing. 9, 1-19.

Paiva, C.M., Franca, G.B., Liu, W.T.H., Rotunno Filho, O.C., 2011. A comparison of experimental energy balance components data and SEBAL model results in Dourados, Brazil. International Journal of Remote Sensing. 32, 1731-1745.

Panday, P.K., Coe, M.T., Macedo, M.N., Lefebvre, P., Castanho, A.D., 2015. Deforestation offsets water balance changes due to climate variability in the Xingu River in eastern Amazonia. Journal of Hydrology. 523, 822-829.

Parker, J.A., Kenyon, R.V., Troxel, D.E., 1983. Comparison of interpolating methods for image resampling. IEEE Transactions on Medical Imaging. 2, 31-39.

Pedlowski, M.A., Dale, V.H., Matricardi, E.A., Silva Filho, E.P., 1997. Patterns and impacts of deforestation in Rondonia, Brazil. Landscape and Urban Planning. 38, 149-157.

Priante Filho, J., Campelo Jr, J.H., Nogueira, J.S., Lyra, G.L., Hayashi, M. Nunes, P.C., Souza, L.S.E., Couto, E.G., Hoeger, W., Raiter, F., Trienweiler, J.L., 2004. Comparison of the mass and energy exchange of a pasture and a mature transitional

tropical forest of the southern Amazon Basin during a seasonal transition. Global Change Biology. 10, 863-876.

Reichstein, M., Falge, E., Baldocchi, D., Papale, D., Aubinet, M., Berbigier, P., Bernhofer, C., Buchmann, N., Gilmanov, T., Granier, A., Grünwald, T., 2005. On the separation of net ecosystem exchange into assimilation and ecosystem respiration: review and improved algorithm. Global Change Biology. 11, 1424-1439.

Restrepo-Coupe, N., da Rocha, H.R., Hutyra, L.R., da Araujo, A.C., Borma, L.S., Christoffersen, B., Cabral, O.M., de Camargo, P.B., Cardoso, F.L., da Costa, A.C.L., Fitzjarrald, D.R., 2013. What drives the seasonality of photosynthesis across the Amazon basin? A cross-site analysis of eddy flux tower measurements from the Brasil flux network. Agricultural and Forest Meteorology. 182, 128-144.

Rocha, H.R., Goulden, M.L., Miller, S.D., Menton, M.C., Pinto, L.D., Freitas, H.C., 2004. Seasonality of water and heat fluxes over a tropical forest in eastern Amazonia. Ecological Applications. 14, 22-32.

Ruhoff, A.L., Paz, A.R., Aragao, L.E.O.C., Mu, Q., Malhi, Y., Collischonn, W., Rocha, H.R., Running, S.W., 2013. Assessment of the MODIS global evapotranspiration algorithm using eddy covariance measurements and hydrological modelling in the Rio Grande basin. Hydrological Sciences Journal. 58, 1658-1676.

Saleska, S.R., Didan, K., Huete, A.R., Rocha, H.R., 2007. Amazon forests green-up during 2005 drought. Science. 318, 612-612.

Sampaio, G., Nobre, C., Costa, M.H., Satyamurty, P., Soares -Filho, B.S., Car 2007. Regional climate change over eastern Amazonia caused by pasture and soybean cropland expansion. Geophysical Research Letters. 34, 1-7.

Santos, C.A.G., da Silva, R.M., Silva, A.M., Neto, R.M.B., 2017. Estimation of evapotranspiration for different land covers in a Brazilian semi-arid region: a case study of the Brígida River basin, Brazil. Journal of South American Earth Sciences. 74, 54-66.

Santos, C.C.D., Nascimento, R.L., Rao, T.V.R. and Manzi, A.O., 2011. Net radiation estimation under pasture and forest in Rondonia, Brazil, with TM Landsat 5 images. Atmósfera. 24, 435-446.

Schuurmans, J.M., Van Geer, F.C., Bierkens, M.F.P., 2011. Remotely sensed latent heat fluxes for model error diagnosis: a case study. Hydrology and Earth System Sciences. 15, 759-769.

Scott, R.L., Watts, C., Payan, J.G., Edwards, E., Goodrich, D.C., Williams, D., Shuttleworth, W.J., 2003. The understory and overstory partitioning of energy and

water fluxes in an open canopy, semiarid woodland. Agricultural and Forest Meteorology. 114, 127-139.

Senay, G.B., Budde, M., Verdin, J.P., Melesse, A.M., 2007. A coupled remote sensing and simplified surface energy balance approach to estimate actual evapotranspiration from irrigated fields. Sensors. 7, 979-1000.

Shuttleworth, W.J., 1989. Micrometeorology of temperate and tropical forest. Philosophical Transactions of the Royal Society of London B: Biological Sciences. 324, 299-334.

Sommer, R., Sa, L.D., Vielhauer, K., Araujo, A.C., Folster, H., Vlek, P.L., 2002. Transpiration and canopy conductance of secondary vegetation in the eastern Amazon. Agricultural and Forest Meteorology. 112, 103-121.

Song, X.P., Huang, C., Saatchi, S.S., Hansen, M.C., Townshend, J.R., 2015. Annual carbon emissions from deforestation in the Amazon Basin between 2000 and 2010. Plos One. 10, 1-21.

Souza Filho, J.D.C., Ribeiro, A., Costa, M.H., Cohen, J.C.P., Rocha, E.J.P., 2006. Seasonal variation of the radiation balance in a northeast Amazonian Rainforest. Brazilian Journal of Meteorology. 3, 318-330.

Souza, P.J.D.O.P., Rocha, E.J.P.D., Ribeiro, A., Souza, E.B.D., 2010. Radiation balance in a soybean ecosystem in the Amazon. Brazilian Agronomic Science Journal. 41, 582-592.

Stark, S.C., Breshears, D.D., Garcia, E.S., Law, D.J., Minor, D.M., Saleska, S.R., Swann, A.L., Villegas, J.C., Aragão, L.E., Bella, E.M., Borma, L.S., 2016. Toward accounting for ecoclimate teleconnections: intra-and inter-continental consequences of altered energy balance after vegetation change. Landscape Ecology. 31, 181-194.

Swann, A.L., Fung, I.Y., Chiang, J.C., 2012. Mid-latitude afforestation shifts general circulation and tropical precipitation. Proceedings of the National Academy of Sciences. 109, 712-716.

Tang, R., Li, Z.L., Chen, K.S., Jia, Y., Li, C., Sun, X., 2013. Spatial-scale effect on the SEBAL model for evapotranspiration estimation using remote sensing data. Agricultural and Forest Meteorology. 174, 28-42.

Timmermans, W.J., Kustas, W.P., Anderson, M.C., French, A.N., 2007. An intercomparison of the surface energy balance algorithm for land (SEBAL) and the two-source energy balance (TSEB) modeling schemes. Remote Sensing of Environment. 108, 369-384.

von Randow, C., Manzi, A.O., Kruijt, B., De Oliveira, P.J., Zanchi, F.B., Silva, R.L., Hodnett, M.G., Gash, J.H.C., Elbers, J.A., Waterloo, M.J., Cardoso, F.L., 2004. Comparative measurements and seasonal variations in energy and carbon exchange over forest and pasture in South West Amazonia. Theoretical and Applied Climatology. 78, 5-26.

Webler, A.D., Gomes, J.B., Aguiar, R.G., De Andrade, N.L., Aguiar, L.J., 2013. Changes in land use and energy partitioning in the southwest of the Amazon. Brazilian Journal of Agricultural and Environmental Engineering. 17, 868-876.

Wright, I.R., Gash, J.H.C., Da Rocha, H.R., Shuttleworth, W.J., Nobre, C.A., Maitelli, G.T., Zamparoni, C.A.G.P., Carvalho, P.R.A., 1992. Dry season micrometeorology of central Amazonian ranchland. Quarterly Journal of the Royal Meteorological Society. 118, 1083-1099.

Yamaguchi, Y., Kahle, A.B., Tsu, H., Kawakami, T., Pniel, M., 1998. Overview of advanced spaceborne thermal emission and reflection radiometer (ASTER). IEEE Transactions on Geoscience and Remote Sensing. 36, 1062-1071.

Yang, J.Y., Mei, X.R., Huo, Z.G., Yan, C.R., Hui, J.U., Zhao, F.H., Qin, L.I.U., 2015. Water consumption in summer maize and winter wheat cropping system based on

SEBAL model in Huang-Huai-Hai Plain, China. Journal of Integrative Agriculture. 14, 2065-2076.

Yang, Y., H. Guan, O. Batelaan, T. R. McVicar, D. Long, S. Piao, W. Liang, B. Liu, Z. Jin, C. T. Simmons., 2016. Contrasting responses of water use efficiency to drought across global terrestrial ecosystems. Scientific Reports. 6, 1-8.

Yang, Y., Shang, S., Jiang, L., 2012. Remote sensing temporal and spatial patterns of evapotranspiration and the responses to water management in a large irrigation district of North China. Agricultural and Forest Meteorology. 164, 112-122.

Zanchi, F.B., Waterloo, M.J., Tapia, A.P., Alvarado Barrientos, M.S., Bolson, M.A., Luizão, F.J., Manzi, A.O., Dolman, A.J., 2015. Water balance, nutrient and carbon export from a heath forest catchment in central Amazonia, Brazil. Hydrological Processes. 29, 3633-3648.

Zeng, N., Yoon, J.H., Marengo, J.A., Subramaniam, A., Nobre, C.A., Mariotti, A., Neelin, J.D., 2008. Causes and impacts of the 2005 Amazon drought. Environmental Research Letters. 3, 1-10.

Zeri, M., Sa, L.D., Manzi, A.O., Araujo, A.C., Aguiar, R.G., von Randow, C., Sampaio, G., Cardoso, F.L., Nobre, C.A., 2014. Variability of carbon and water fluxes following climate extremes over a tropical forest in southwestern Amazonia. Plos One. 9, 1-12.

Zhang, Q., Cheng, Y.B., Lyapustin, A.I., Wang, Y., Xiao, X., Suyker, A., Verma, S., Tan, B., Middleton, E.M., 2014. Estimation of crop gross primary production (GPP): I. impact of MODIS observation footprint and impact of vegetation BRDF characteristics. Agricultural and Forest Meteorology. 191, 51-63.

Figure Legends:

Figure 1. Map showing the study area and the location of the flux tower used in this study.

Figure 2. Land-cover map of the study area for (a) 6/16/2004 and (b) 7/5/2005. The arrows show the fish bone pattern of deforestation in the Brazilian Amazon.

Figure 3. Spatial distribution of (a) albedo, (b) net radiation (Rn), (c) soil heat flux (G), (d) sensible heat flux (H), (e) evapotranspiration (ET), and (f) evaporative fraction (EF) in the study area on 6/16/2004 and 7/5/2005.

Figure 4. (a) Incoming shortwave radiation (K↓) (W m-2), (b) air temperature (Tair) (ºC) and (c, d) precipitation (PPT) (mm) measured at the JBR flux tower. K↓ and Tair were measured between 7:00-17:00 local time. PPT was measured over 30 days prior the ASTER scenes acquisition, between 5/17/2004-6/15/2004 and 6/5/2005 and 7/4/2005.

Figure 5. Illustration exemplifying some of the plots used to extract the SEBAL estimates for different land cover types in the study area. The white boxes show the 12-pixel window, and the coordinates represent the central location for each box. The false-color composite (R3G2B1) was obtained through the ASTER image from 6/16/2004.

Figure 6. Magnitudes of (a) albedo, (b) net radiation (Rn) (W m-2), (c) soil heat flux (G) (W m-2), (d) sensible heat flux (H) (W m-2), (e) evapotranspiration (ET) (mm day-1), and (f) evaporative fraction (EF) for different land cover types in the study area.

Figure 7. Relative variation (%) in albedo, net radiation (Rn), soil heat flux (G), sensible heat flux (H), evapotranspiration (ET) and evaporative fraction (EF) for each situation of land cover change (primary tropical forest (PF) to pasture (PA), primary tropical forest (PF) to agriculture (AG) and primary tropical forest (PF) to secondary succession forest (SF)).

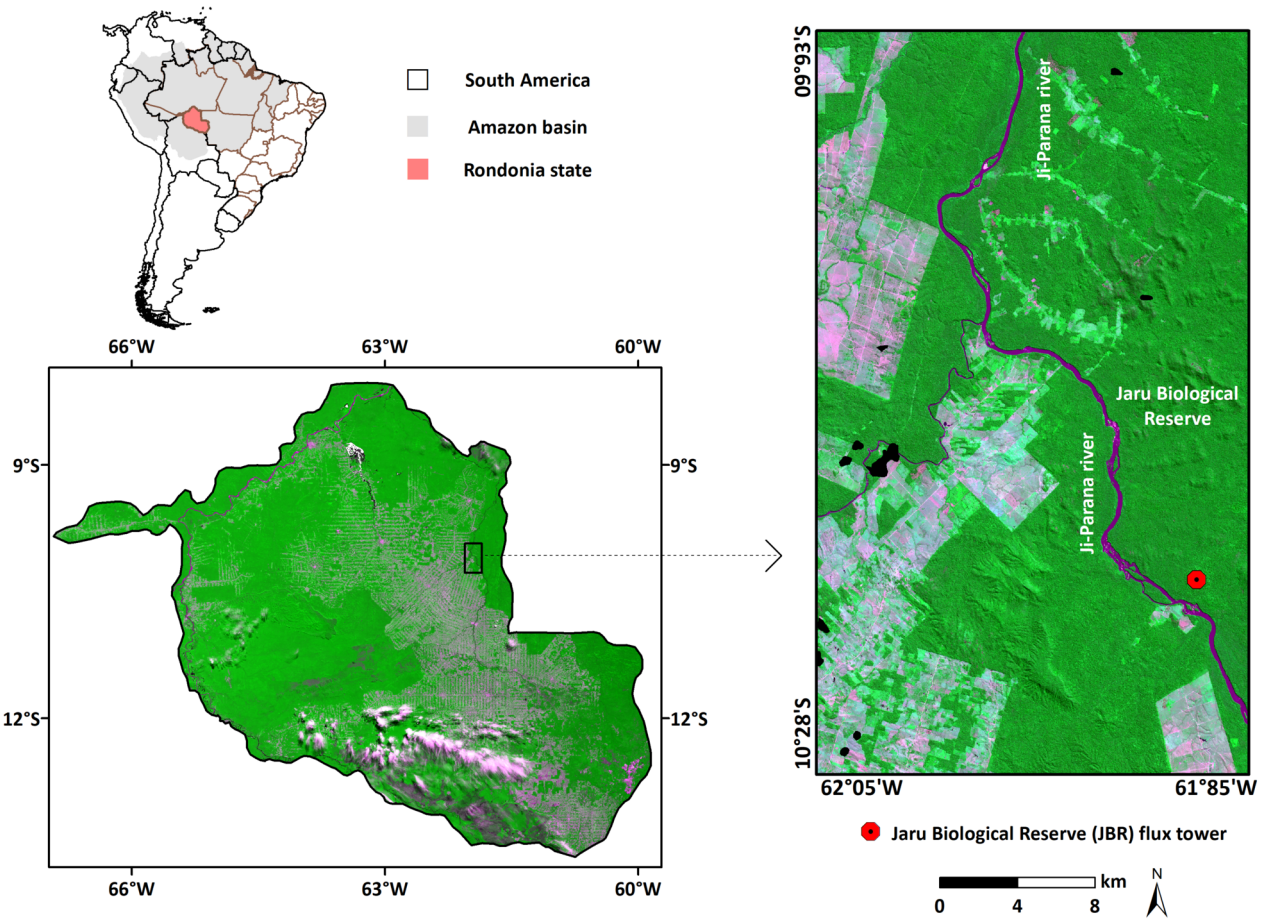

ECO_2126_F1.tif

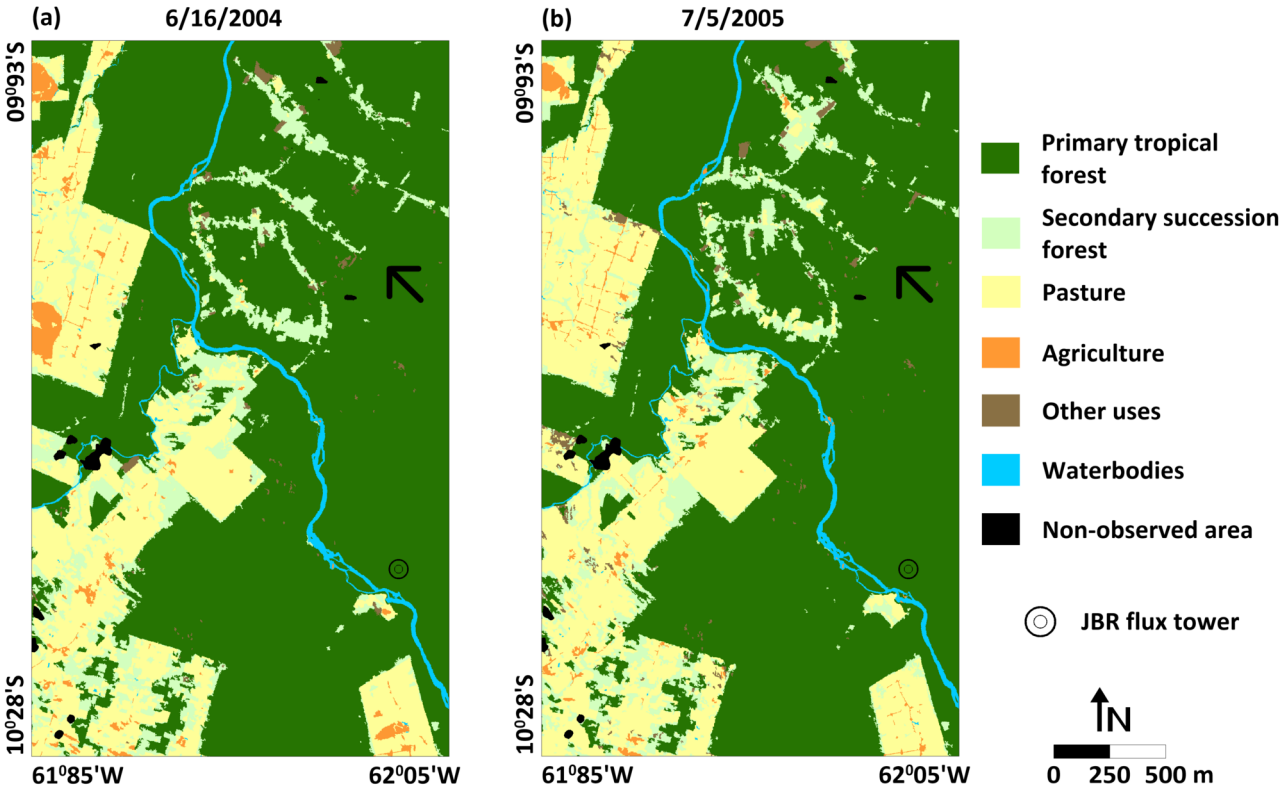

ECO_2126_F2.tif

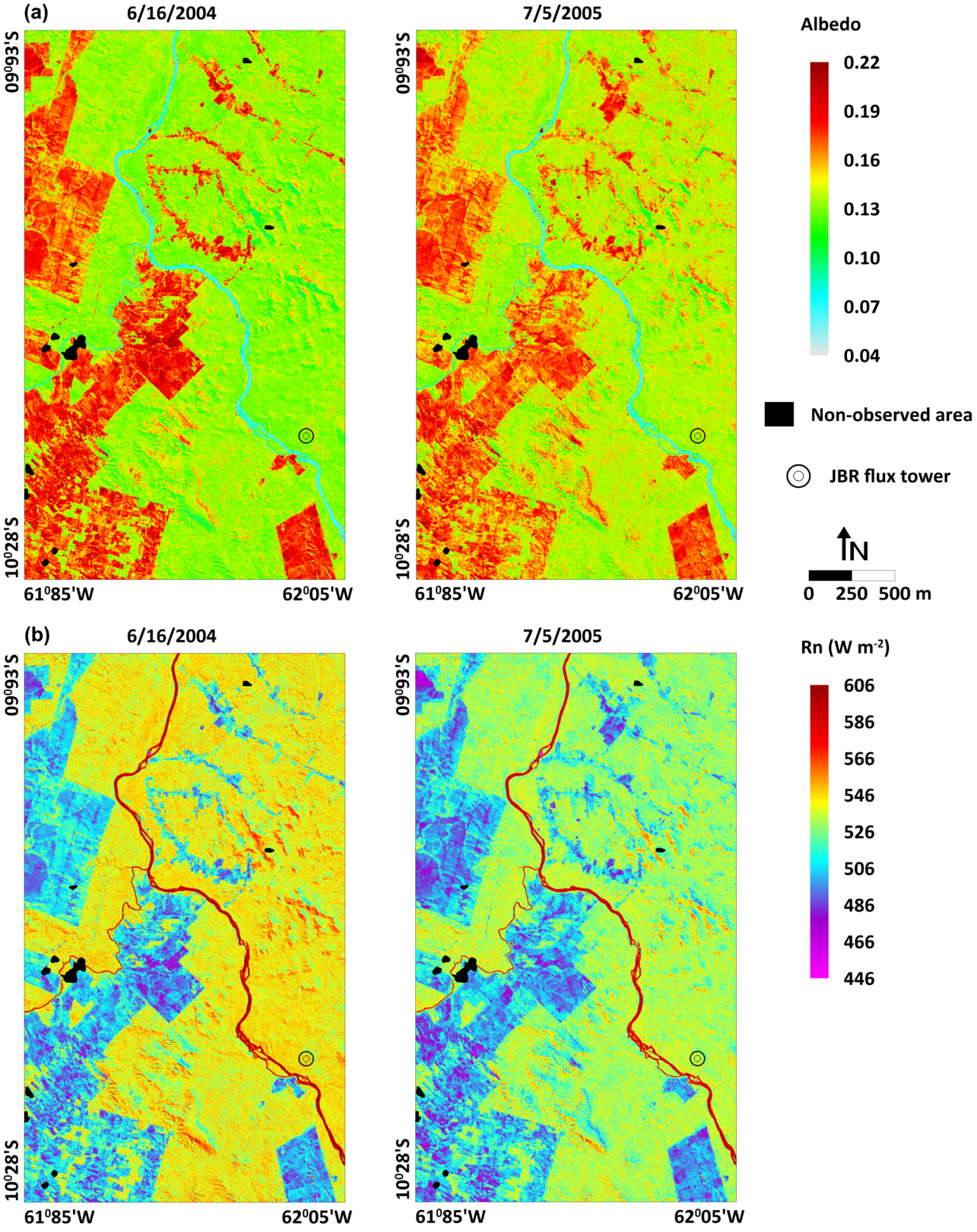

ECO_2126_F3-1.tif

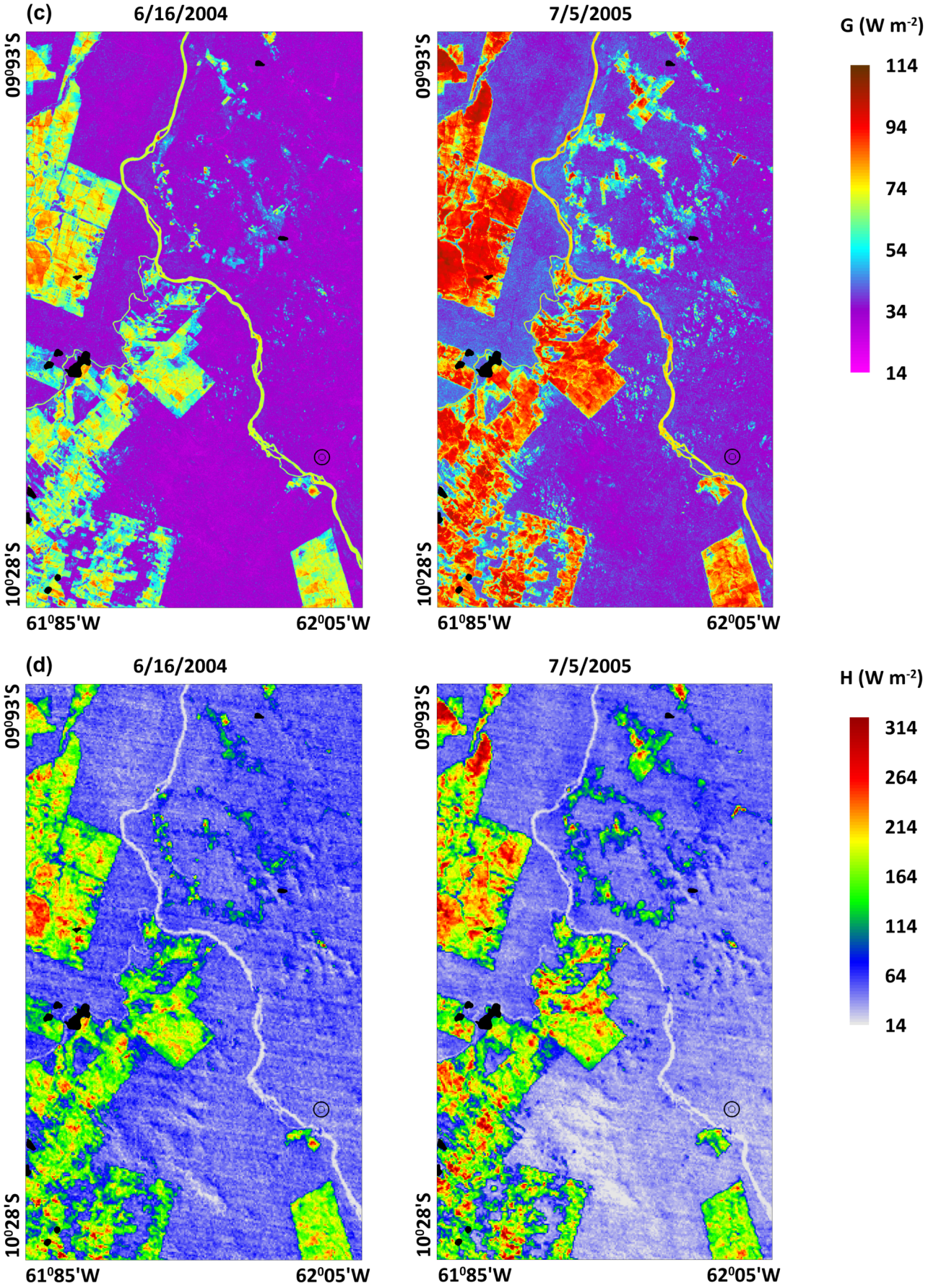

ECO_2126_F3-2.tif

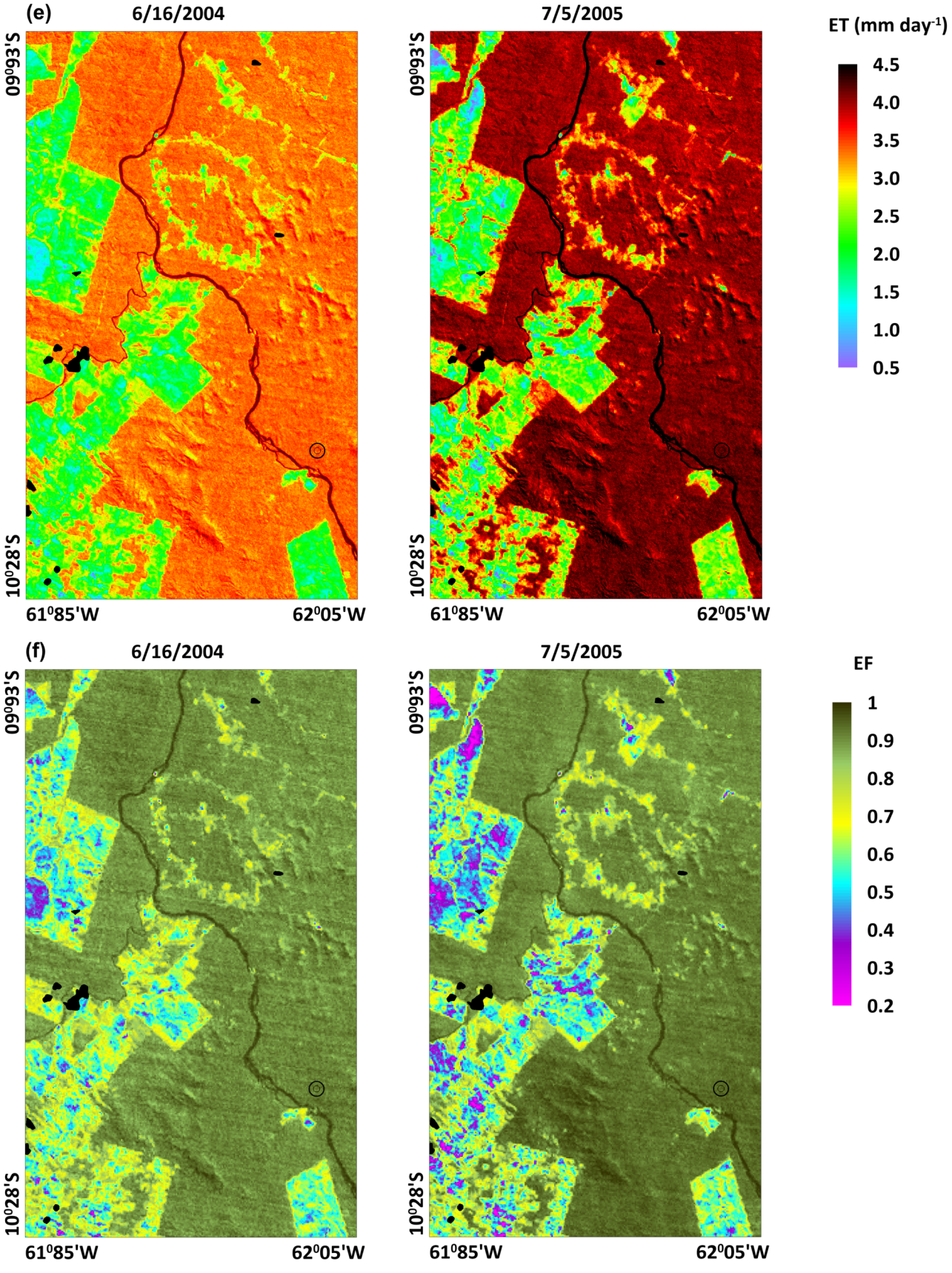

ECO_2126_F3-3.tif

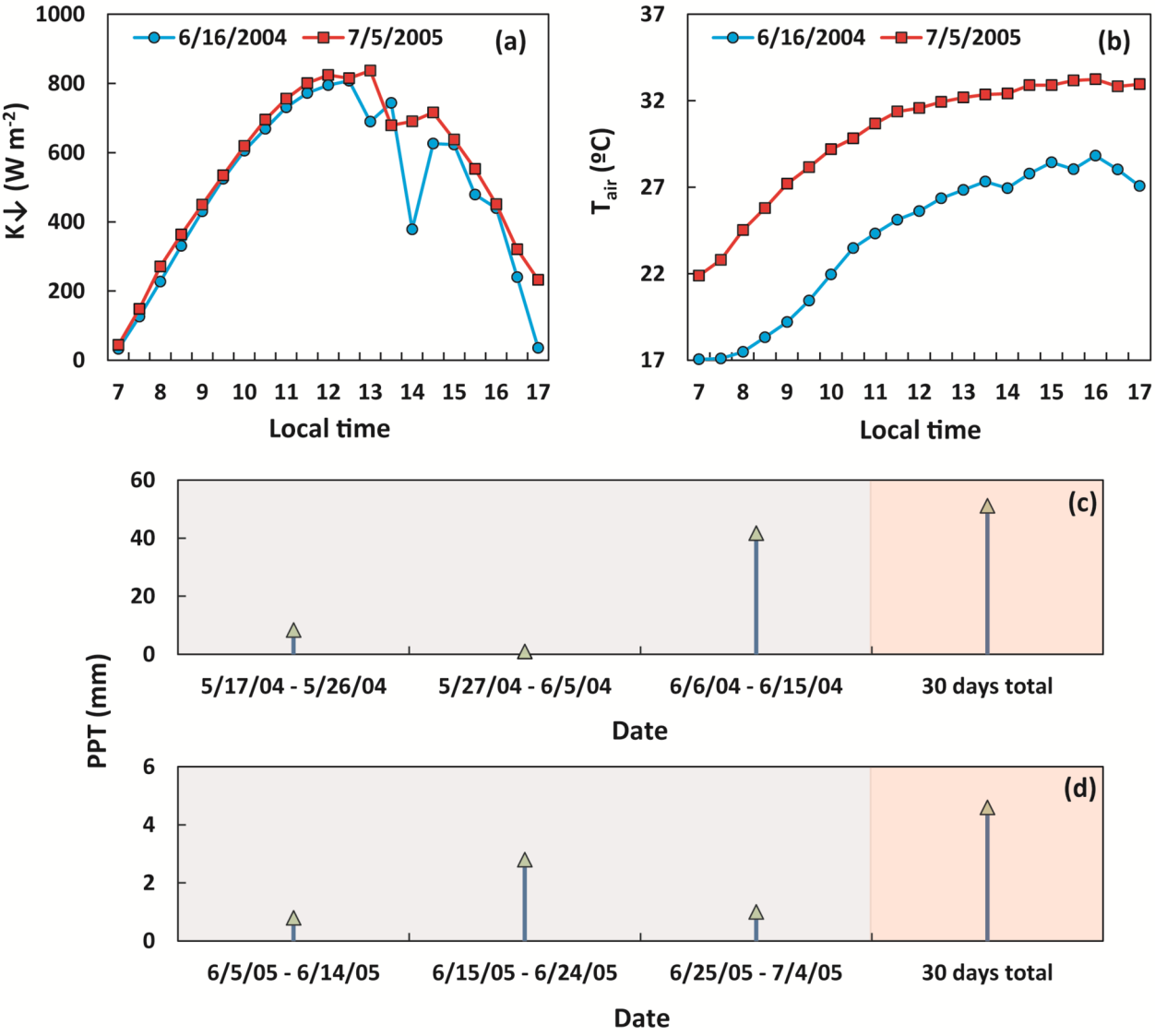

ECO_2126_F4.tif

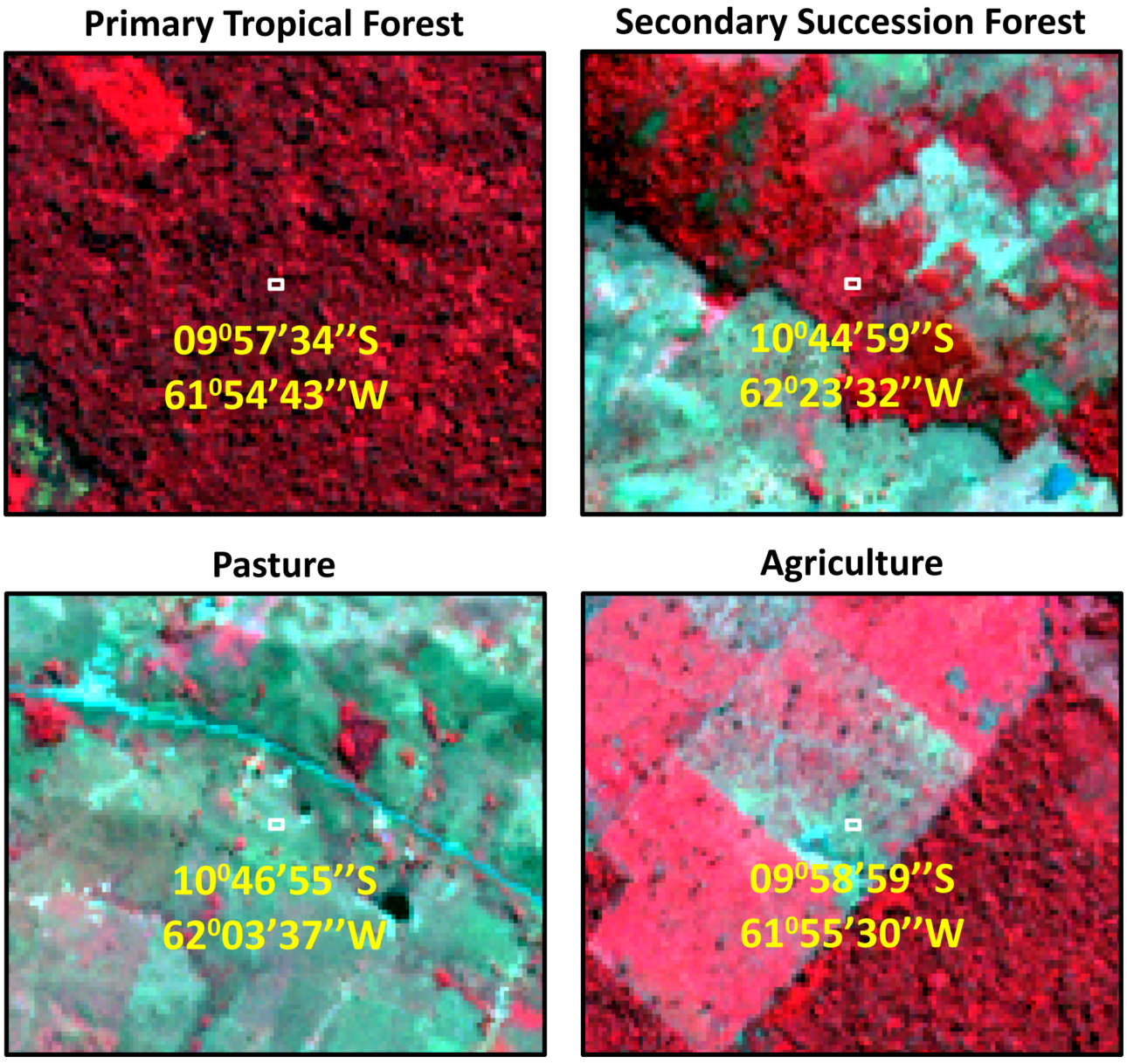

ECO_2126_F5.tif

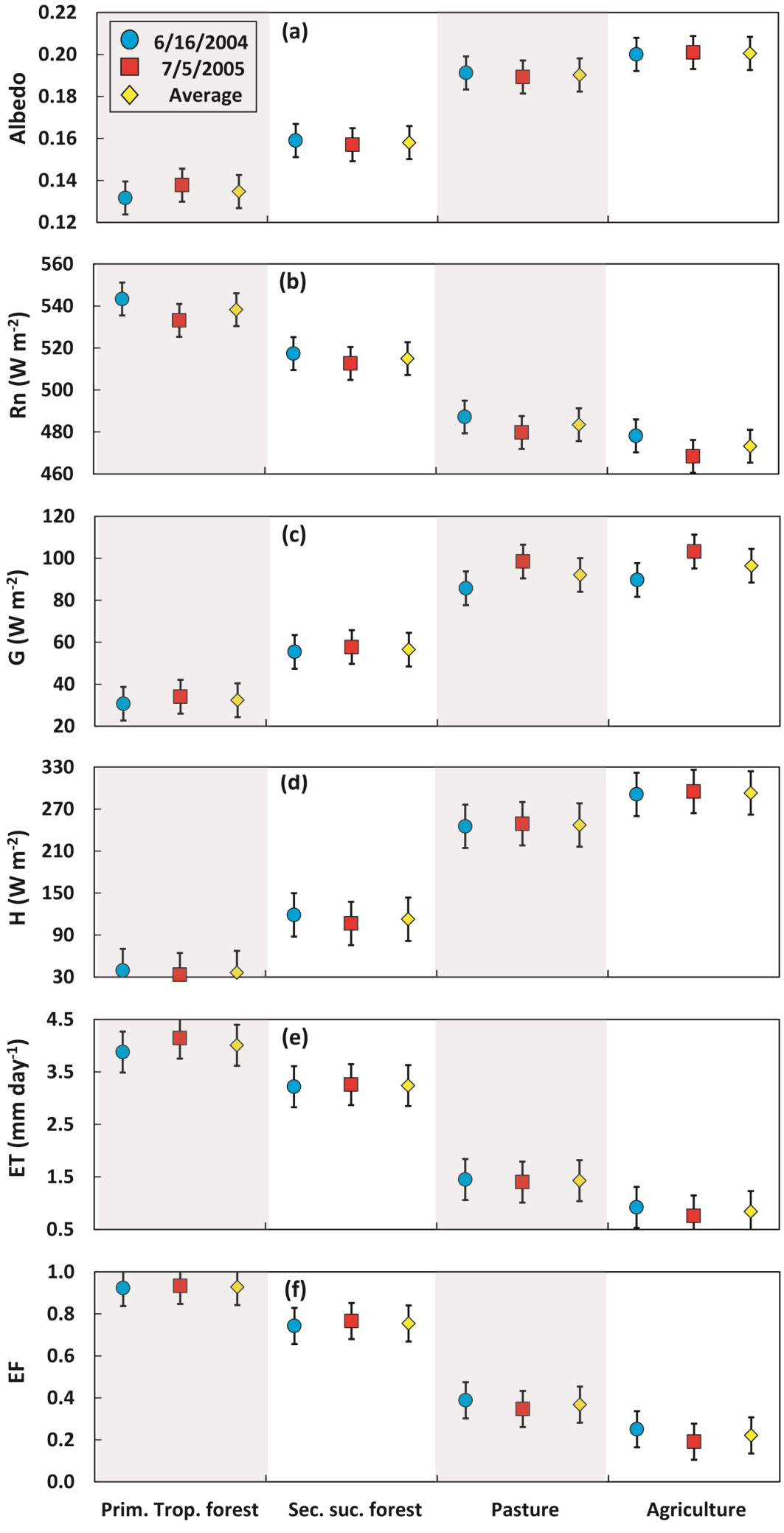

ECO_2126_F6.tif

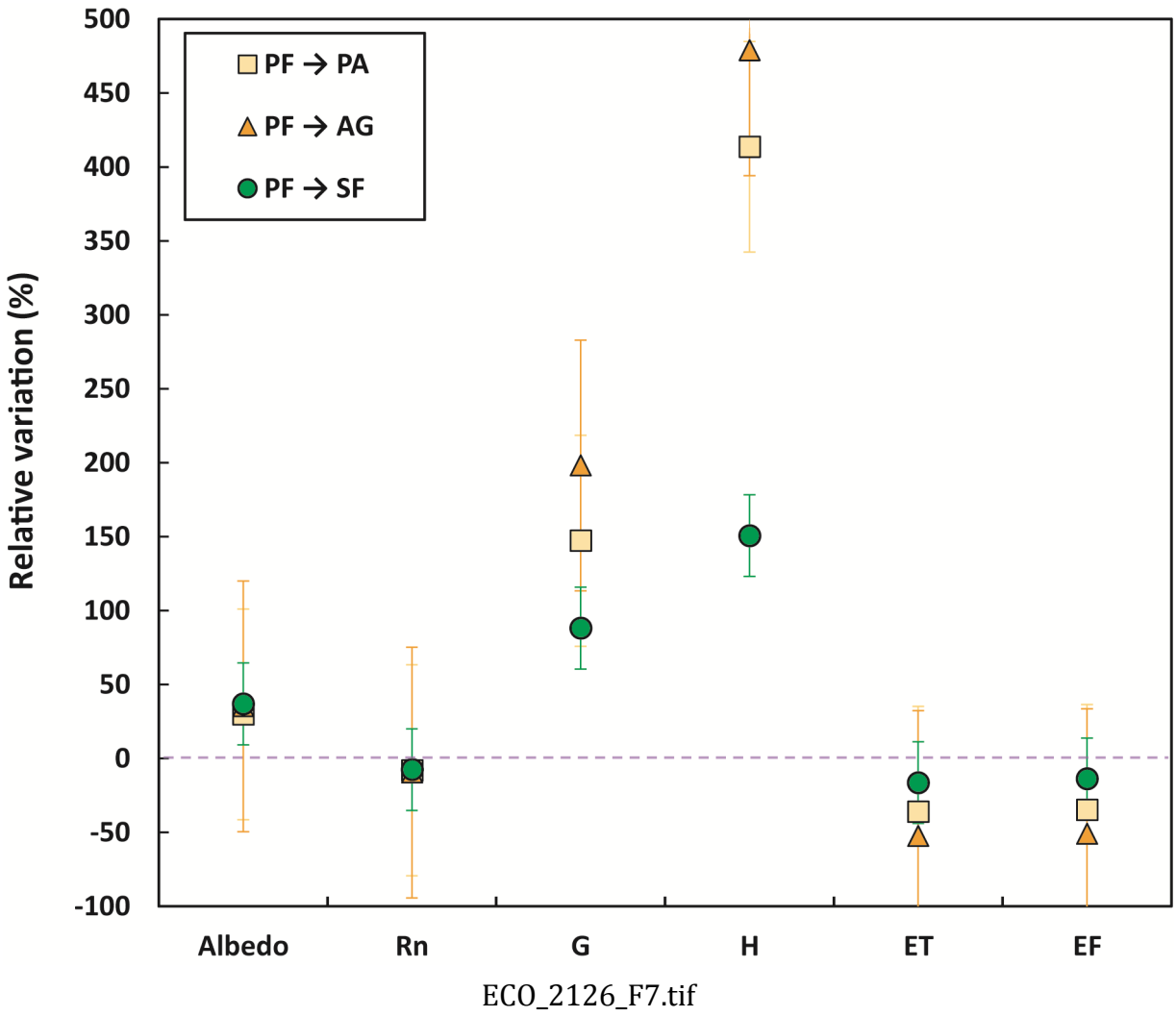

ECO_2126_F7.tif